



Mohamed Khider University of Biskra
Faculty of exact sciences and natural and life sciences
Material sciences department

MASTER MEMORY

Material sciences
Physics
Energrtic physics and Renewable Energies

Réf. : Entrez la référence du document

Prsentedd by:
AMMARI NOUMIDIA

Le :

Study of solar blind photodetector based on beta gallium oxide ($\beta\text{-Ga}_2\text{O}_3$)

Jury:

Abdeslam Nora Amele

MCB University of Biskra

President

Meftah Afak

Prof University of Biskra

Supervisor

Nouadji Malika

MCB University of Biskra

Examiner

AcademicYear:2022/2023

Dedication:

*I dedicate this work to my lovely parents, my friends and my
brothers.*

Acknowledgments:

This thesis would not have been possible without my advisor, Pr, Meftah Afak, person to whom I wish to convey my solidest gratitude and profound respect and to whom I am indebted to for this whole thesis work. It was a great experience to work with him. She provided me with constant guidance, encouragements, thanks alone isn t enough to cover all the situation that you helped me and all the efforts that she made to achieve this dissertation. Thank you for everything and for your kind treatment .I would like to thank also all the professors in the field of material sciences.Finally, I would like to thank the members of the jury, Dr.Laznek Samira and Dr.Abdsalam Nora amele who have kindly accepted to read and examine this work.

ملخص:

تعد اجهزة الكشف عن الاشعة فوق البنفسجية من الاجهزة الواعدة و التي يتنافس العلماء و الباحثين في تطويرها و خصوصا تلك القائمة على اكسيد الغاليوم . دراستنا في هذه المذكرة سوف تتمحور حول كاشف ضوئي β -IZTO / Ga_2O_3 . وذلك بسبب تقنيات التصنيع الغير مكلفة والحساسية الفعالة اتجاه الاشعة فوق البنفسجية. من اجل دراسة خصائصها قبل تصنيعها قمنا بعمل محاكاة لهذا الجهاز بواسطة Silvaco-Atlas، حيث اعتمدنا في بنائه على الوصلة شوتكي. تم دراسة هذا الجهاز في الظروف التالية : الجهاز معرض لمصدر ضوئي LED بثلاثة اطوال موجية مختلفة 255nm, 385nm, 500nm . دراستنا تنقسم الى جزئين حيث : في الجزء الاول من الدراسة تمت دراسة الخواص التالية للجهاز : الخاصية تيار- جهد (I-V) والاستجابة و كذلك وقت الاستجابة . اما في الجزء الثاني سوف ندرس تأثير تخفيض العيوب العميقة منها او الضحلة ووجد ان هذه الاخيرة تؤثر و بشكل مباشر على وقت الاستجابة و بالتالي اداء الكاشف.

الكلمات المفتاحية : اكسيد الغاليوم ، كاشف ضوئي حساس للاشعة فوق البنفسجية، Silvaco-Atlas

Abstract:

In recent years, the solar-blind photodetectors based on β -Ga₂O₃ are attractive due to their simple fabrication process and its photodetection performance. Our study is about InZnSnO₂ (IZTO)/ β -Ga₂O₃ solar blind Schottky barrier diode photodetector (PhD). It was realized successfully by Silvaco-Atlas simulation. The first part of our study is to expose this device to light source (LED) (255 nm, 385 nm and 500 nm) with a power density of 1 mW/cm² and it was simulated J-V, responsivity, response time characteristics and compared with measurement. In the second part of our study is study the effect of reducing trap densities (deep and shallow trap) on performance of the photodetector. When we decrease in deep trap densities, we notice that the saturation zone current is decrease. However, when the decreasing shallow traps densities, we notice that The decay time was shorter (~0.019s for $E_T = 0.55$ eV). However, it was be slower when the trap is deeper because we find his value for $E_T = 0.74$ eV is ~0.38 s and for $E_T = 1.04$ eV is ~0.099s. So, this indicates that the shallowest traps had the dominant influence ($E_T = 0.55$ eV) on the persistent photoconductivity phenomenon. Furthermore, with decreasing trap densities, this PhD can be considered as a self-powered solar-blind photodiode (SBPhD).

Key words : Beta gallium oxide, solar blind photodetector, Silvaco-Atlas.

Table of contents

Dedecation.....	i
Acknowledgments.....	ii
ملخص.....	iii
Abstract.....	iv
Table of contents.....	v
List of figures.....	x
List of tables.....	xiii
List of abriviations	xiv
General introduction	1
CHAPTER I : Fundamental properties of beta gallium oxide β-Ga₂O₃ .	
I.1.Introduction.....	4
I.2.History of gallium oxide	4
I.3.Gallium oxide.....	8
I.3.1. Polymorphs	8
I.4.Beta gallium oxide β-Ga₂O₃	11
I.5.Fundamental properties of β-Ga₂O₃.....	12
I.5.1.Crystal structure of β-Ga₂O₃	12
I.5.2.Electronic tructure of β-Ga₂O₃	13
I.5.3.Main defects on β-Ga₂O₃	14

<i>1.5.3.1. Intrinsic defects</i>	15
<i>1.5.3.1.1. Oxygen vacancies</i>	15
<i>1.5.3.1.2. Gallium vacancies</i>	15
<i>1.5.3.1.3. Oxygen interstitial (O_i) and Ga interstitials (Ga_i)</i>	16
<i>1.5.3.2. Extrinsic defects:</i>	16
<i>1.5.3.2.1. Hydrogen interstitials (H_i) and substitution (H_o)</i>	16
<i>1.5.4. Doping in β-Ga_2O_3</i>	17
<i>1.5.4.1. N-type doping</i>	17
<i>1.5.4.2. P-type doping</i>	18
<i>1.5. Electrical properties</i>	19
<i>1.5.1. Energy bandgap of β-Ga_2O_3</i>	19
<i>1.5.2. Carrier mobility</i>	20
<i>1.5.3. Free electron concentration and resistivity</i>	22
<i>1.5.5.4. Breakdown electrical field</i>	24
<i>1.5.6. Optical properties</i>	26
<i>1.5.6.1. Optical bandgap</i>	26
<i>1.5.6.2. reflection index</i>	27
<i>1.5.6.3. Transmission and absorption</i>	28
<i>1.5.7. Thermal properties</i>	30
<i>CHAPTER II : Background of β-Ga_2O_3 solar blind photodetectors:</i>	
<i>II.1. Introduction</i>	33
<i>II.2. Background and motivation of studying solar blind photodetector based on beta gallium oxide</i>	34
<i>II.3. Operating principle of Photodetector</i>	36

II.4. Basic Parameters of UV photodetectors	36
II.4.1. Dark current	36
II.4.2.Responsivity	36
II.4.3.Response time	37
II.4.4. Specific detectivity	37
II.4.5. Quantum efficiency	38
II.4.6.Gain	38
II.4.7. Linear dynamic range	38
II.5. β-Ga₂O₃ solar-blind UV photodetectors	39
II.5.1.Photoconductors	39
II.5.2. MSM photodiode	41
II.5.3.PN photodiode	41
II.5.4.P-I-N photodiode	43
II.5.5.Schottky photodiode	44
II.6. The basic Concept of Schottky Barrier Diode	45
 CHAPTER III: Study of IZTO/β-Ga₂O₃ Photodetector based on Schottky Barrier Diode by Silvaco-Atlas.	
III.1.Introduction	51
III.2.Silvaco-Atlas	52
III.2.1. A brief of how a structure is built and simulated	53
III.2.1.Mesh	54
III.2.1.2.Region	56
III.2.1.3.Contacts	57
III.2.1.4.Doping	58

III.2.1.5. Material.....	59
III.2.1.6. Models	60
III.2.1.7. Numerical method selection.....	61
III.2.1.8. Solution specification.....	62
III.2.1.9. Data Extraction and Plotting	63
III.3. Device structure and physical models	63
III.3.1. Device structure	63
III.3.2. Optical and Electrical Properties of IZTO Thin Film	65
III.3.3. The used physical models.....	67
III.3.3.1. standard concentration dependent mobility model.....	68
III.3.3.2. Parallel field mobility model.....	69
III.3.3.3. Shockley–Read–Hall (SRH) model	69
III.3.3.4. Auger recombination.....	70
III.3.3.5. Selberherr’s impact ionization.....	71
III.3.3.6. Universal Schottky Tunneling (UST) model.....	72
III.3.3.7. Thermionic emission model	72
III.3.3.8. Fermi–Dirac statistics.....	73
III.4. Results and discussion.....	73
III.4.1. Current density-Voltage (J-V) characteristic.....	73
III.4.2. Responsivity.....	75
III.4.3. Response time	77
III.4.4. The effect of bulk traps	79
III.4.4.1. The effect on(J-V) characteristic	79
III.4.4.2. The effect on response time	81

<i>III.5.Conclusion</i>	83
<i>Final conclusion</i>	84
<i>References</i>	86

List of figures:

Figures of chapter I:

Figure I.1: Number of research studies on Ga ₂ O ₃ as a function of time	5
Figure I.2: Absorption Edge of Pure β-Ga ₂ O ₃ measured in 1965	6
Figure I.3: Photograph of a 4-in. diameter single-crystalline Ga ₂ O ₃ wafer.....	7
Figure I.4: Schematic device structures. (a) Schematic cross section of a Ga ₂ O ₃ field-plated MOSFET, (b) schematic cross section of a Ga ₂ O ₃ MESFET and (c) schematic illustration of a prototype GaN/β-Ga ₂ O ₃ p-n junction photodetector	7
Figure I.5: Chart illustrating transformation relationships among gallium oxide polymorphs.....	10
Figure I.6: Comparison of breakdown field of various	11
Figure I.7: Crystal structure of β-Ga ₂ O ₃	12
Figure I.8: The band gap of β-Ga ₂ O ₃	13
Figure I.9: Intrinsic and extrinsic defects in β-Ga ₂ O ₃	15
Figure I.10: Formation energies of the different point defects in β-Ga ₂ O ₃ plotted against the Fermi energy for oxygen poor conditions	16
Figure I.11: Column chart of band gap on different materials.....	19
Figure I.12: Variation of electron mobility in β-Ga ₂ O ₃ with temperature	20
Figure I.13: Relationship between mobility and carrier concentration for Sn-doped β-Ga ₂ O ₃ films.....	21
Figure I.14: The resistivity of the β-Ga ₂ O ₃ films with different Sn concentrations	23
Figure I.15: Electric breakdown fields corresponding to bandgap of major WBG semiconductor material	24
Figure I.16: Comparison of breakdown voltage and specific on-state resistance in candidate materials for high power electronics	25
Figure I.17: Some examples of coloration of β-Ga ₂ O ₃ crystals	26
Figure I.18: Spectra for refractive index <i>n</i> of β-Ga ₂ O ₃ thin film and substrate	27
Figure I.19: The transmittance spectra of β-Ga ₂ O ₃ crystals	27

Figure I.20: The absorption spectra of β -Ga ₂ O ₃ single crystal	29
Figure I.21: Temperature dependence of the thermal conductivity of β -Ga ₂ O ₃ in different crystallographic directions.	30

Figures of chapterII:

Figure II.1: Subdivision diagram of the ultraviolet light region.	33
Figure II.2: (a) Schematic structure of a photoconductor[1]. (b) Spectral responses of the photoconductors based on β -Ga ₂ O ₃ films prepared at various temperatures. (c) Current-voltage (<i>I-V</i>) characteristics of the β -Ga ₂ O ₃ photodetector in dark, under 365 and 254 nm light radiation. (d) Experimental curve and fitted curve of the current rise and decay process to 254 nm illuminations. (e) Schematic diagram illustrating the carrier transport mechanism in the β -Ga ₂ O ₃ photodetector.	40
Figure II.3 : Schematic structure of MSM photodetector	41
Figure II.4: Schematic structure of p-n heterojunction diode	43
Figure II.5: Schematic structure of an example of solar blind photodetector based on pin photodiode: solar blind p-ZnO:LiNO ₃ /i-Ga ₂ O ₃ /n-Ga ₂ O ₃ :Si	44
Figure II.6 : Schematic structure of schottky diode	45
Figure II.7 : A Schottky barrier formed by a metal of high work function contacting a n-type semiconductor.	46

Figures of chapter III:

Figure III.1: Simulation flow diagram of Silvaco-Atlas.....	52
Figure III.2: Command group and statements layout for a Silvaco Atlas file.....	54
Figure III.3 : Example of a mesh Profile in a simulated device	55
Figure III 4 : Device region specification.	57
Figure III.5 : A schematic representation of the β -Ga ₂ O ₃ Schottky barrier diode (SBD) structure. ...	64
Figure III.6 : Main optical properties of IZTO thin film	66

Figure III.7 :Avalanche breakdown process in a reverse-biased PN junction.....	71
Figure III.8 : The J–V characteristic at reverse bias simulated at different wavelengths (solid lines) of the fully transparent β -Ga ₂ O ₃ SD UVPhD compared to measurements (symbols).Each wavelength corresponds to an LED light source of 1 mW/cm ²	74
Figure III.9 : Responsivity versus wavelength at different reverse voltage (simulation—solid lines) (measurements—symbols).	76
Figure III.10 : Photocurrent density versus light power density for 255 nm and at –1 V.	77
Figure III.11 : The time-dependent photoresponse under pulsed illumination of 255 nm at –1 V.	78
Figure III.12 : The effect of bulk trap reduction (electron traps) present in the band gap energy of β -Ga ₂ O ₃ , (a) ET= 0.55 eV, (b) ET= 0.74 eV and (c) ET= 1.04 eV on the J-V characteristics.....	80
Figure III.13 : The effect of the reduction defects (one by one), (a) ET= 0.55 eV, (b) ET= 0.74 eV and (c) ET= 1.04 eV on Photocurrent density versus light power density of β -Ga ₂ O ₃ solar blind UV-PD.....	81
Figure III.14 : The effect of defect reduction on time-dependent photoresponse under short-pulsed illumination of 255 nm at –1 V: (a) ET= 0.55 eV, (b) ET= 0.74 eV and (c) ET= 1.04 eV	82

List of tables:

Tables of chapter I:

Table I.1: Ga ₂ O ₃ polymorphs[12] (note: For the figures of each polymorph I took them from the reference[15]).	9
Table I.2: Electric properties measured by Hall effect measurement [51].	22
Table I.3: Thermal properties of β-Ga ₂ O ₃ [69].	29

Tables chapter III:

Table III.1 : Physical input material parameters in the simulation process.	64
Table III.2 : Input trap parameters in the simulation process.	65
Table III.3 : Main IZTO properties for simulation :	67

List of abbreviations:

<i>UV</i>	<i>Ultraviolet region</i>
<i>MSM</i>	<i>Metal-semiconductor-metal photodetector</i>
<i>UWBG</i>	<i>Ultra-wide bandgap</i>
<i>PDs</i>	<i>Photodetectors</i>
<i>TFT</i>	<i>Thin film transistor</i>
<i>MOSFET</i>	<i>Metal oxide semiconductor field effect</i>
<i>SBD</i>	<i>Schottky barrier diode</i>
<i>SBHs</i>	<i>Schottky barrier heights</i>

Introduction

Ultraviolet (UV) detection has attracted considerable attention, owing to its versatile applications in civilian infrastructures, military facilities, and scientific research[1]. It is an important component of solar radiation[2].

The UV spectral region is widely established to occupy the spectral interval of $\lambda = 400\text{--}10$ nm. It is commonly divided into the following subdivisions: UV-A (for wavelengths between 400 and 320 nm), UV-B (for wavelengths between 320 and 280 nm), UV-C (for wavelengths between 280 and 200 nm), and far UV (for wavelength between 200 and 10 nm)[1]. Most of the UV light from the sun, it is absorbed by the atmospheric ozone layer. Due to this absorption, there are less ultraviolet radiations with wavelengths at 220 ~ 280 nm surface on the earth, this range of solar radiation named the solar-blind ultraviolet regime. Thus, solar-blind UV photodetectors have the high-precision detection and strong anti-interference ability, even exposed to sunlight[3]. Therefore, it has been considered that solar-blind photodetectors play an important part in missile tracking, inter-satellite communications, and ozone monitoring[4].

There are many structure types of solar-blind photodetectors up to now, e.g., photoconductor, metal-semiconductor-metal (MSM) photodetectors , Schottky-type photodetectors , heterojunction-type photodetectors , and so on. The features of photodetectors with different structures are also different, among which, solar blind photodetectors based on Schottky diode is the purpose of the dissertation.

A large number of semiconductors have been employed as the active layer in solar-blind photodetectors[4]. Wide bandgap compound semiconductors made a huge advance and extended functionality of photodetector devices due to their high voltage operation, fast switching behaviour, and thermal stability. Wide bandgap materials, such as GaN, InGaN and SiC were used in many applications in the last decade. Nowadays, research has concentrated on ultra-wide bandgap (UWBG) semiconducting materials of which the energy gap exceeds 4 eV. There are several UWBG materials that attract particular attention, including AlGaN, AlN, diamond, and $\beta\text{-Ga}_2\text{O}_3$ [3]. $\beta\text{-Ga}_2\text{O}_3$ has excellent intrinsic properties such as a wide bandgap of ~ 4.8 eV and the absorption peak that locates in the solar-blind ultraviolet region, a high breakdown electrical field of ~ 8 MV/cm and a high saturation velocity of 10^7 cm/s. It has also a low cost and a large scale produced material

compared to GaN, InGaN and SiC. However, this material has a serious drawback of developing p-type, thus hindering its application in bipolar devices[4],[5].

Currently, $\beta\text{-Ga}_2\text{O}_3$ is mainly used in unipolar devices such as SBD, MOSFET, TFT and field emission. For SBDs (Schottky Barrier Diodes), the control of Schottky barrier heights (SBHs) at metal/semiconductor interfaces is a critically important technique to design switching properties of semiconductor, which means it requires high work function metals for Schottky contact with $\beta\text{-Ga}_2\text{O}_3$ [6],[5].

In this dissertation, solar blind photodetector based on $\beta\text{-Ga}_2\text{O}_3$ is numerically modelled by Silvaco-Atlas software. This device structure is a Schottky diode. The top contact is InZnSnO (IZTO), the n layer is $\beta\text{-Ga}_2\text{O}_3$ which are make together a schottky contact ,and the bottom contact is indium tin oxide (ITO). The aim of this work is to study the device characteristics including : the J-V characteristic under illumination , the responsivity, the sensitivity, the response time that describes the speed response of the photodetector. This in order to examine the performance of the device. In addition, we will study how the reduction of the bulk defects improves the performance of the Schottky diode -IZTO/ $\beta\text{-Ga}_2\text{O}_3$ photodetector.

The dissertation is organized as follows:

Chapter I presents the electrical, optical, thermal and electronic properties of $\beta\text{-Ga}_2\text{O}_3$.

Chapter II summarizes the main types of solar blind photodetector based on $\beta\text{-Ga}_2\text{O}_3$, the basic parameters of a photodetector and the principals of a Schottky barrier diode .

Chapter III explains the software used in this thesis (Silvaco-Atlas), the results of modelling SBD(IZTO/ $\beta\text{-Ga}_2\text{O}_3$) and the effect of bulk traps on its performance.

CHAPTER I:

**Fundamental properties of
beta gallium oxide $\beta\text{-Ga}_2\text{O}_3$**

I.1 Introduction:

The electronics and the computing that we use today is due to the Silicon technology invented 50 years ago. But as all good things come to an end, it is time for Silicon technology in semiconductor industry to end[7] . So in order to satisfy the demand of the fast development of electrical power, industrial control, automotive electronics, and consumer electronics industries, which requires high-performance power semiconductor devices[8], wide bandgap semiconductors such as Silicon carbide (SiC) and Gallium nitride (GaN) are being pursued to replace Si in power electronic devices[9].

Recently, a new wide bandgap semiconductor (WBG), beta gallium oxide ($\beta\text{-Ga}_2\text{O}_3$), has begun to receive worldwide scientific and technological attention because of its unique properties, rapid materials development[10],[11] and availability of economically intrinsic substrates[12] which makes it well suited for power electronics, solar blind photodetectors and deep ultraviolet optoelectronics and sensing[12] applications[13].

This chapter gives a general introduction about $\beta\text{-Ga}_2\text{O}_3$. We will discuss about the fundamental properties of $\beta\text{-Ga}_2\text{O}_3$ (crystal structure, electrical, optical and thermal properties), because knowing and understanding them well enable us to aid in the development of advanced technologies in the future and solve current issues confronting this material[12].

I.2 History of gallium oxide:

Although gallium oxide is the subject of much recent research activities around the world for both optical and electrical applications, the interest in Ga_2O_3 dates back many years[14].

Figure I.1 is shown number of research studies on Ga_2O_3 as a function of time:

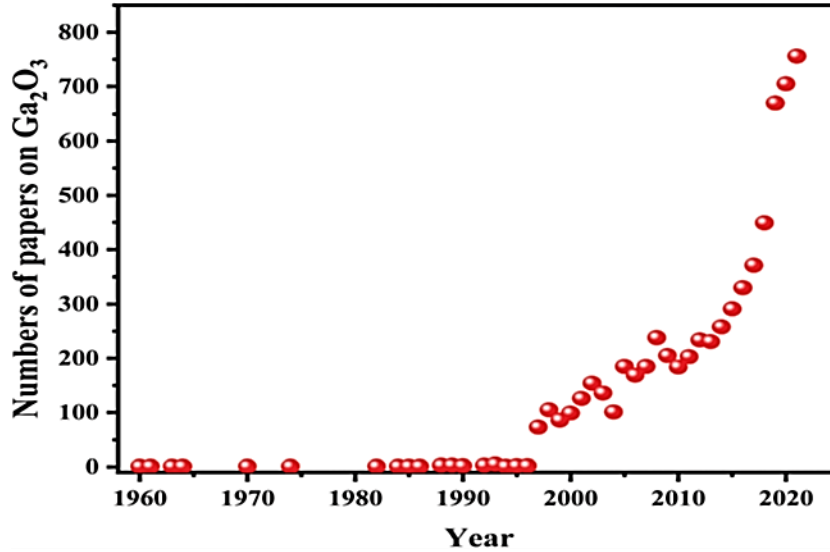


Figure I.1: Number of research studies on Ga₂O₃ as a function of time [15].

The number of publications on Ga₂O₃ has accelerated in recent years, as is evident from **figure I.1**, due to the interest in electronic and photonic devices with capabilities beyond the existing technologies. There has been a healthy balance of experimental and theoretical investigations of the properties of the Ga₂O₃ system[16]. The history of Ga₂O₃ dates back to 1875 when Lecoq de Boisbaudran described newly discovered element gallium and its compounds[17]. In 1952, the phase equilibria of the Al₂O₃-Ga₂O₃-H₂O system was first reported[18], in which the polymorphs (same composition but different crystal structures depending on how it was grown[19]) of Ga₂O₃ and their regions of stability were also identified[16].

The investigations of Ga₂O₃ in the period of 1960s–1980s were mostly based on materials with poor crystallinity or even in amorphous forms, though some attempts for making Ga₂O₃ single crystals started to appear. Most of the early publications mainly focused on the basic physical properties and chemical synthesis of β -Ga₂O₃[20], for example, **figure I.2**

shows the measured optical absorption edge for $\beta\text{-Ga}_2\text{O}_3$ in a U.S. Air Force sponsored study in 1965 [14].

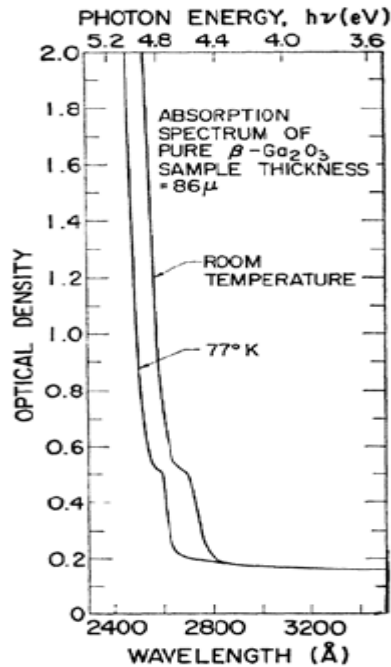


Figure I.2: Absorption Edge of Pure $\beta\text{-Ga}_2\text{O}_3$ measured in 1965[14].

These optical characteristics are consistent with more recent studies. However, The electrical characteristics were only recently analyzed since they are highly dependent on the crystal quality, and the initial crystals were full of defects[21],[14].For a while in 1970s, Ga_2O_3 was well known and used as an insulator on GaAs wafers[14]. From the 1990s to 2010s, significant progress has been achieved in successful growth of a bulk single crystal of high quality and large size, for example, a large Ga_2O_3 single crystal with size up to 70 mm \times 50 mm \times 3 mm was realized by the edge defined film-fed growth (EFG) method. **figure I.3** shows a single crystal grown by the EFG technique[20].

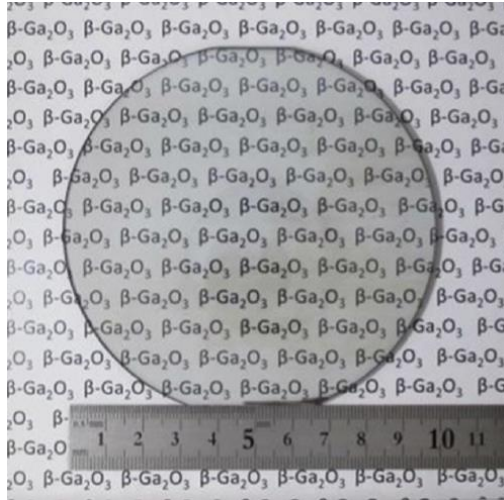


Figure I.3: Photograph of a 4-in. diameter single-crystalline Ga_2O_3 wafer[20], [22].

Triggered by the growth of large-size bulk crystals, Ga_2O_3 based device research, including Ga_2O_3 based field-effect transistors (FETs), Schottky barrier diodes (SBDs), and solar blind ultraviolet detectors, has been experiencing a rapid rise in the past few years. Some representative device structures are shown in **figure I.4** [20].

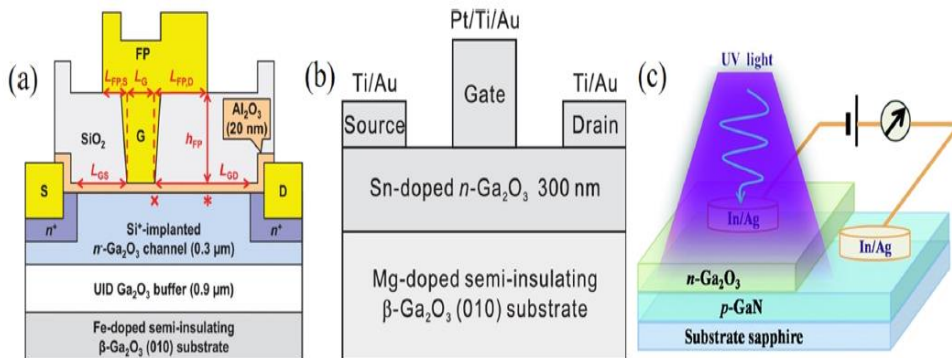


Figure I.4: Schematic device structures. (a) Schematic cross section of a Ga_2O_3 field-plated MOSFET, (b) schematic cross section of a Ga_2O_3 MESFET and (c) schematic illustration of a prototype $\text{GaN}/\beta\text{-Ga}_2\text{O}_3$ p-n junction photodetector [20].

In 2008, solar-blind UV photodetectors based on Ga₂O₃ single crystal substrates were initially developed since that, Ga₂O₃ solar-blind UV photodetectors have been broadly studied in the types of metal-semiconductor-metal (MSM) photodetectors, Schottky barrier photodetectors, and p-n or n-n junction photodiodes using Ga₂O₃ bulk crystals, films, and micro/nanostructures[20]. Today, gallium oxide is considered a key technology as it is primarily a WBG semiconductor. But it is not unique in this respect. There are several other well-known WBG semiconductors in use today such as GaAs, GaN, SiC and ZnO. So, what makes Ga₂O₃ a special WBG semiconductor [14].

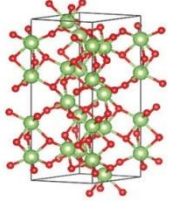
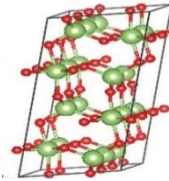
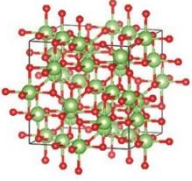
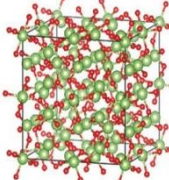
I.3 Gallium oxide:

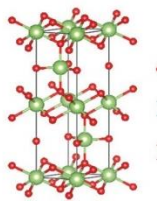
Gallium oxide (Ga₂O₃) is an emerging ultrawide bandgap (UWBG) semiconducting material[13]. It belongs to transparent conducting oxide (TCO) materials[12]. It has a bandgap of about 4.4–5.3 eV, which results from the different polymorphs of Ga₂O₃ with different structure symmetry and the optical anisotropy along different crystalline orientations [13].

I.3.1. Polymorphs:

In general, there are five different polymorphs labelled as $\alpha, \beta, \gamma, \delta$ and ϵ for Ga₂O₃ single crystal[23]. Each polymorph can exhibit differences between band alignment, in the crystal space group, the coordination number of Ga⁺³ ions. In addition, each polymorph exhibits its Ga₂O₃ phases under specific conditions. These polymorphs, which belong to the family of Ga₂O₃, have different structure forms, electrical and optical characteristics in real-life applications[12]. Table below is shown some properties of each polymorph. Of these, the monoclinic phase β -Ga₂O₃ is the stable form under normal conditions of temperature and pressure (from room temperature up to the melting point of about 1800 °C).

Table I.1: Ga₂O₃ polymorphs[12] (**note:** For the figures of each polymorph I took them from the reference[15]).

<i>Structure</i>	<i>Group space</i>	<i>Lattice parameters</i>	<i>Band gap</i>
<p>α-Ga₂O₃</p> 	R-3c	$a=4.9825 \text{ \AA}$ $c=13.433 \text{ \AA}$ $\alpha=\beta=90^\circ$ $\gamma=120^\circ$	5.3 eV
<p>β-Ga₂O₃</p> 	C2/m	$a=12.214 \text{ \AA}$ $b=3.0371 \text{ \AA}$ $c=5.7981$ $\alpha=\gamma=90^\circ$ $\beta=103.83^\circ$	4.8 eV
<p>γ-Ga₂O₃</p> 	Fd-3m	$a=b=c=8.45 \text{ \AA}$ $\alpha= 90.79^\circ$ $\beta= \gamma= 89.21^\circ$	7 Ev
<p>δ-Ga₂O₃</p> 	Ia3	$a=9.401 \text{ \AA}$ $\alpha=\beta=\gamma=90^\circ$	Not available

$\epsilon\text{-Ga}_2\text{O}_3$	Pna21	a=5.0463	4.9 eV
			

In addition being unaffected even by concentrated acids such as hydrofluoric acid[24]) consequently it has the best thermal stability, while the other four phases are metastable and are apt to transform to $\beta\text{-Ga}_2\text{O}_3$ under certain conditions (above 600 °C, 1 h or more[25]). Therefore, at present, most studies focus on $\beta\text{-Ga}_2\text{O}_3$ [8], [18]. The transformation relationships among these five phases are shown in **figure I.5** [8]. In this chapter we will focus on the monoclinic structured $\beta\text{-Ga}_2\text{O}_3$ polymorph.

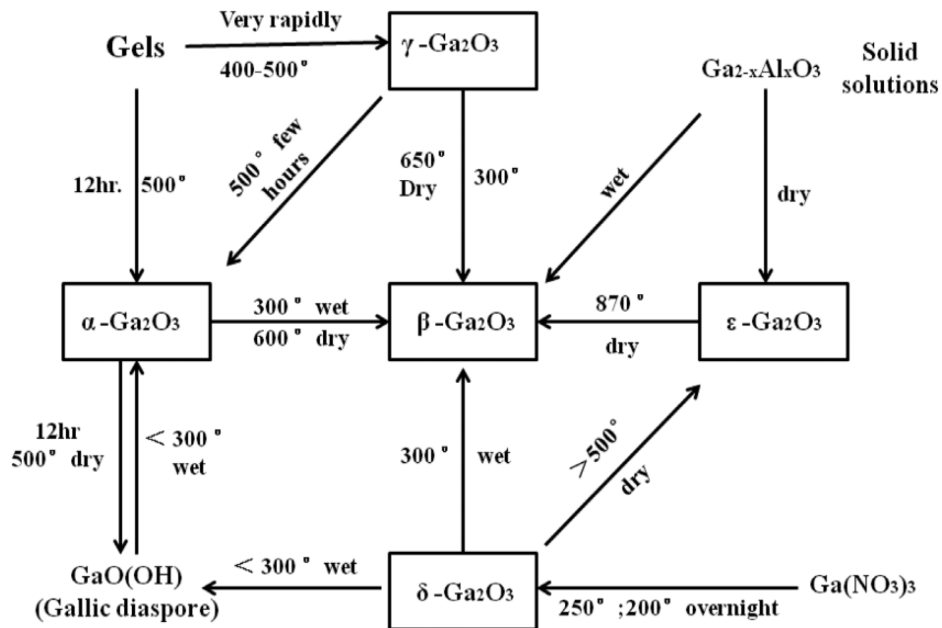


Figure I.5: Chart illustrating transformation relationships among gallium oxide polymorphs[25], [26].

I.4 Beta gallium oxide $\beta\text{-Ga}_2\text{O}_3$:

Beta gallium oxide is an n-type semiconductor that has exceptionally large band gap, in excess of ~ 4.5 eV [27]. It is one of the five structures of Ga_2O_3 single crystal with a monoclinic structure [8] which has promising applications due to its properties, such as its high thermal and chemical stability [28], its wide bandgap and its large breakdown electric field of ~ 8 MV/cm (much higher than others, like GaN (~ 5 MV/cm) and SiC (~ 3 MV/cm))[29], as can be seen in **figure I.6**:

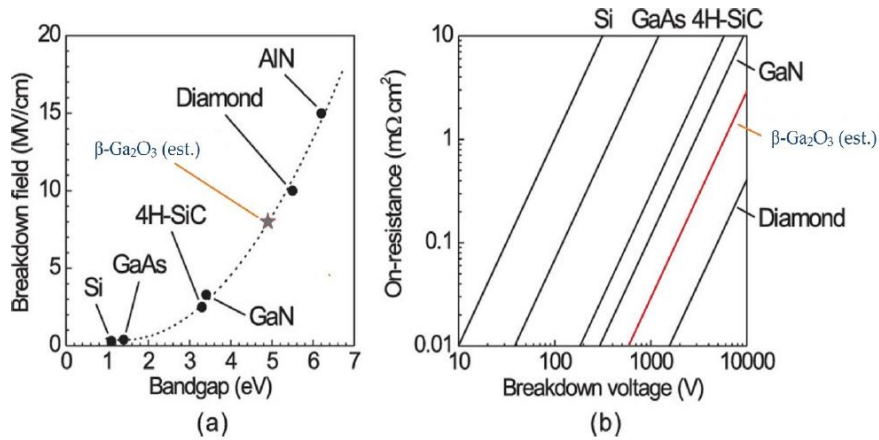


Figure I.6: Comparison of breakdown field of various [29].

Additionally, $\beta\text{-Ga}_2\text{O}_3$ is one of the few wide-band-gap semiconducting oxides that remains transparent well into the ultraviolet (UV) [30]. It has a unique transparency from the visible into the UV region, it is a very promising candidate for optoelectronic devices operating at short wavelength, where the other TCOs have poor transparency[24] . In the other hand ,the ease of fabrication of large area native substrates, control of carrier concentration, and inherent thermal stability also motivate the development of $\beta\text{-Ga}_2\text{O}_3$ based devices [20].

I.5 Fundamental properties of $\beta\text{-Ga}_2\text{O}_3$

I.5.1 Crystal structure of $\beta\text{-Ga}_2\text{O}_3$:

$\beta\text{-Ga}_2\text{O}_3$ crystallizes in the monoclinic space group $C2/m$ [31] with lattice parameters $a=12.214 \text{ \AA}$, $b=3.0371 \text{ \AA}$, $c=5.7981 \text{ \AA}$, $\alpha=\gamma=90^\circ$, $\beta=103.83^\circ$ [12]. The unit cell structure of $\beta\text{-Ga}_2\text{O}_3$ is shown in **figure I.7**.

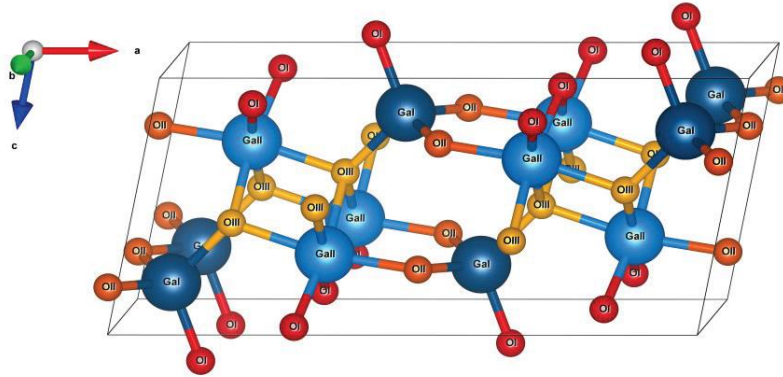


Figure I.7: Crystal structure of $\beta\text{-Ga}_2\text{O}_3$ [32].

The unit cell as presented in figure above contains 20 atoms consisting of crystallographically inequivalent Ga^{+3} and O^{-2} atoms [33]. Ga atoms are coordinated tetrahedrally (GaI) and octahedrally (GaII), while O atoms are coordinated threefold (OI and OIII) and fourfold OII. The tetrahedrally coordinated (GaI) shares bonds with one OI ion with a bond length of 1.835 \AA , one OIII ion with a bond length of 1.833 \AA , and two OII ions with a bond length of 1.863 \AA . The octahedrally coordinated (GaII) ions share bonds with two OI ions with a bond length of 1.937 \AA , one OII ions with a bond length of 1.937 \AA , and three OIII ions (one with 2.005 \AA and two within the bc -plane with 2.074 \AA) [20].

This combination of the tetrahedral and octahedral Ga atoms with threefold and fourfold oxygen atoms creates a complex and interconnected network of Ga-O bonds in $\beta\text{-Ga}_2\text{O}_3$ that leads to an anisotropy of physical, optical and electrical[18].

I.5.2 Electronic structure of $\beta\text{-Ga}_2\text{O}_3$:

The fundamental electrical and optical characteristics of a material are defined by its electronic band structure. With this knowledge, we can conclude a proper device design with a desired functionality[33]. The **figure I.8** has shown the electronic band structure of $\beta\text{-Ga}_2\text{O}_3$.

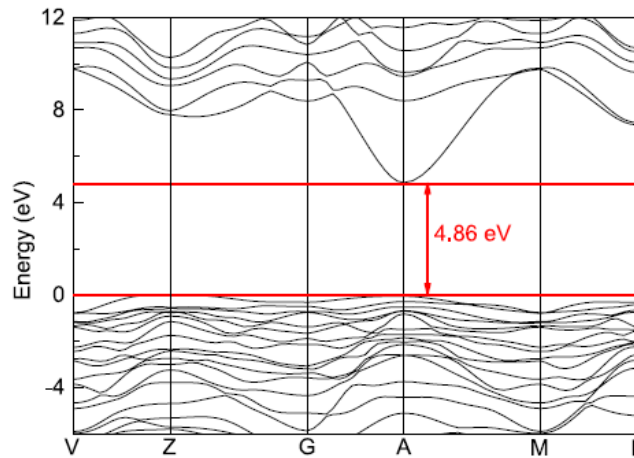


Figure I.8: The band gap of $\beta\text{-Ga}_2\text{O}_3$ [34].

There is a general consensus that $\beta\text{-Ga}_2\text{O}_3$ has a direct bandgap of ~ 4.86 eV [34] (though with a slightly smaller indirect bandgap of 4.83 eV [20]), but due to the weakness of the indirect transitions and the small energy difference between indirect and direct gaps, it is effectively a direct bandgap material [35].

The performance of wide-bandgap oxides is intimately related to the behavior of electrons in the lowest-energy unoccupied (conduction band) states and holes in the highest-energy occupied (valence band) states [36]. The maximum of the valence band is defined as zero energy level [37]. The valence band is mainly formed by O 2p orbitals and are characterized by small dispersion, large effective masses, and high density of states. These are common

features among WBG oxides [36]. Materials with this feature favor the formation of localized oxygen hole polarons [38]; because the very small dispersion of the valence band maximum (VBM) results in a very high effective hole mass[33]. Holes tend to form localized small polarons i.e., localized holes trapped by local lattice distortions[18]. Therefore, the very small dispersion of the valence band maximum (VBM) results in a very high effective hole mass and consequently in a very low hole mobility making a possible p-type conductivity impractical [33].

The conduction band (above the zero energy level) is mainly formed by Ga 4s orbitals [37], giving rise to a dispersive band with a low electron effective mass [20].

I.5.3 Main defects on $\beta\text{-Ga}_2\text{O}_3$:

Although $\beta\text{-Ga}_2\text{O}_3$ has been fabricated by several methods, there are inevitable defects in $\beta\text{-Ga}_2\text{O}_3$ which significantly play important roles in the properties of the material and the optical and electronic properties of the $\beta\text{-Ga}_2\text{O}_3$ based devices so it is essential to identify and characterize these defects[15],[39]. Intrinsic defects, which are native defects, only involve the atoms of the host crystal, and include oxygen vacancies (V_o), gallium vacancies (V_{Ga}), oxygen interstitials (O_i), and gallium interstitials (Ga_i). Extrinsic defects involve impurity atoms, which originate from unintentional doping during the material synthesis process, such as H, Si, or intentional doping with other donor impurities, such as Sn, Ge, Mg, and Fe [39].

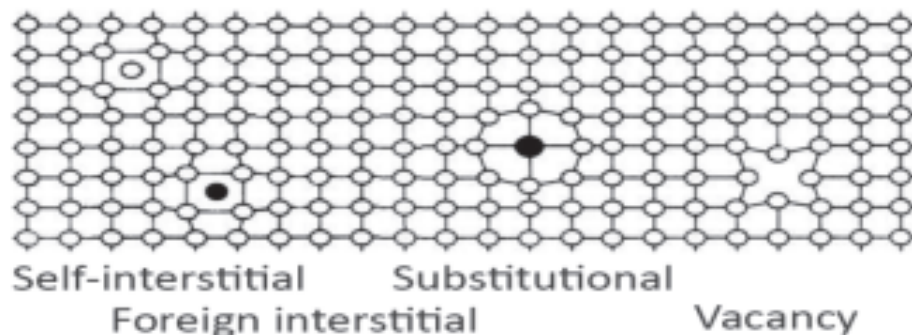


Figure I.9: Intrinsic and extrinsic defects in $\beta\text{-Ga}_2\text{O}_3$ [32].

I.5.3.1. Intrinsic defects :

I.5.3.1.1. Oxygen vacancies:

As a definition of “vacancy” we can say that a vacancy is a missing atom from a normally occupied site (we can call it also a “Schottky defect”)[40]. So the oxygen vacancies are the missing oxygen atoms from a normally occupied site in the lattice structure of $\beta\text{-Ga}_2\text{O}_3$.

It is found that the formation energies for oxygen vacancies (V_o), in $\beta\text{-Ga}_2\text{O}_3$ is more than 1 eV, which indicates that V_o acts as a deep donor and thus can not contribute to the observed un-intentional n -type conductivity[39],[41].

I.5.3.1.2. Gallium vacancies:

Because Ga has three valence electrons, the missing Ga atom leaves three O dangling bonds that can accept electrons. So the V_{Ga} reduce the free-electron concentration . V_{Ga} commonly acts as a deep acceptor defect that can compensate donors [39].

I.5.3.1.3. Oxygen interstitial (O_i) and Ga interstitials (Ga_i):

If an oxygen or gallium atom in a $\beta\text{-Ga}_2\text{O}_3$ crystal is not in its proper site, then it is self-interstitial (O_i and Ga_i)[39]. Gallium and oxygen interstitials play the roles of donor and acceptor respectively in principle. They have some effects on n-type conduction and p-type conduction[15]. However, it is found that interstitial defects always have high formation energies (even more than 2.5 eV) which makes these defects less likely to be present[39],[42].

I.5.3.2. Extrinsic defects:

I.5.3.2.1. Hydrogen interstitials (H_i) and substitution (H_o):

In general, residual hydrogen impurities from the growth ambient are suggested as shallow donors which is contributing significantly to the native n-type conductivity in $\beta\text{-Ga}_2\text{O}_3$; this is due to The low formation energy of hydrogen impurities. Hydrogen can occupy different locations, e.g., interstitial, Ga vacancy or Oxygen vacancy[38], [39]. Extrinsic and intrinsic defects in $\beta\text{-Ga}_2\text{O}_3$ form several traps distributed over the whole bandgap (as we are shown in **figure I.10**) such traps affect the electrical properties of $\beta\text{-Ga}_2\text{O}_3$ [43].

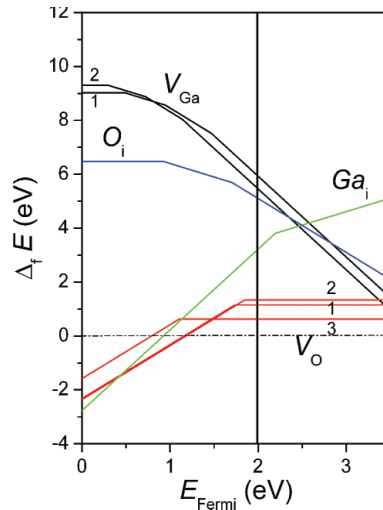


Figure I.10: Formation energies of the different point defects in $\beta\text{-Ga}_2\text{O}_3$ plotted against the Fermi energy for oxygen poor conditions [42].

I.5.4 Doping in $\beta\text{-Ga}_2\text{O}_3$: As with any new wide bandgap materials technology, the control of conductivity through doping is the key to realizing device applications[18],[44]

I.5.4.1. N-type doping:

N-type doping of $\beta\text{-Ga}_2\text{O}_3$ can be achieved by intentional doping with compounds like Si, Ge, and Sn as shallow donors. These shallow donors replace the atoms of the host crystal and have one more valence electron than the atom it replaces. The extra electrons can be easily

activated into the conduction band minimum (CBM) as free carriers, resulting a significant increase in conductivity [39].

It is found that these compounds have a low activation energy (E_a) that depends on the doping concentration (N_d) because we noted that E_a decreases with an increase in N_d . So this low activation energy prove the easy activated of dopant elements. Therefore, the low E_a promotes Si, Ge, and Sn to be common n-type dopants in β -Ga₂O₃ [39].

When we use Si, Sn, and Ge as dopants, a wide range of free carrier concentration (n) from 10^{16} cm^{-3} up to 10^{19} cm^{-3} which meet the basic requirements of high-performance devices, also a peak mobility of $152 \text{ cm}^2/\text{V s}$ have been achieved[20],[15].

I.5.4.2. P-type doping:

Contrary to the ease of n-type doping, the creation of enough positive mobile carriers (holes) contributed to p-type conductivity is the most serious limitation for the development of β -Ga₂O₃ devices even though there are some potential acceptor dopants: magnesium (Mg), zinc (Zn), and beryllium (Be)[45],[13]. This is mainly limited by:

- ✓As we mentioned earlier, the valence band states are made up of O 2p states and are slightly dispersed, resulting in large effective mass for holes and high valence band densities of states. Therefore, p-type conduction either intrinsic or extrinsic does not look feasible due to the tendency of holes to form localized polarons [46],[14].
- ✓The high formation energy of the native acceptors that produce holes, such as cation vacancies[13].
- ✓ The low energy of hole-killer native defect donors, such as cation interstitials and anion vacancies [39],[47].
- ✓It has been found that the potential acceptor dopants, such as that we mentioned earlier, create deep levels in β -Ga₂O₃ due to the flat nature of valence band, self-trapping of holes (polaron formation), and high hole effective mass[38].

From these reasons, hole conductive in β -Ga₂O₃ seems to be hardly realized. If p type conductivity in β -Ga₂O₃ is not possible, as it seems, this would be a major barrier for the Ga₂O₃ technology because without p-type conductivity p-n junctions will not be possible. P-N junction is one of the fundamental building blocks of electronic devices. Without p-type conductivity all electronic devices become majority-carrier type leading to unipolar devices only. Minority-carrier devices are an important part of power electronics as in the Si and SiC technologies. Although high breakdown voltage devices can be fabricated using only majority carrier semiconductors, low on-resistance is difficult to achieve without minority carriers [14].

I.5.5 Electrical properties:

Electrical properties of β -Ga₂O₃ constitute a key factor in defining the operation and functionality of a fabricated electronic device, therefore, their exploration and understanding is of high importance. These properties include all features that affect the flow and control of the electrical current [33]. Here are some of the key electrical properties of β -Ga₂O₃ that are relevant to its use in electronic devices:

I.5.5.1. Energy bandgap of β -Ga₂O₃:

Band gap defines one of the most important electrical properties of β -Ga₂O₃. The band gap β -Ga₂O₃ is ~ 4.8 eV, which is far greater than the band gap of other semiconductor materials, like Silicon (1.1 eV), SiC (3.26 eV) and GaN (3.4 eV)[37] which makes it suitable for high-power and high-temperature electronic applications [13].

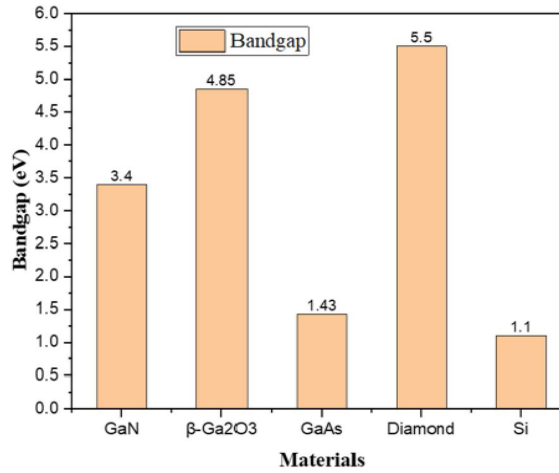


Figure I.11: Column chart of band gap on different materials[48].

As we mentioned before, research has confirmed that $\beta\text{-Ga}_2\text{O}_3$ is an indirect bandgap material, but due to the weakness of the indirect transitions and the small energy difference between indirect and direct gaps, it is effectively a direct bandgap material [35].

I.5.5.2. Carrier mobility:

Carrier mobility is one of the key parameters to perform efficient electronic power devices based on this material [49]. The mobility is defined as the ability of electrons (or charged carrier) to move through a solid material (e.g. metals or semiconductors), under the influence of an electric field [50]. The electron mobility of $\beta\text{-Ga}_2\text{O}_3$ is far lower than that of other wide bandgap semiconductors, such as 4H-SiC ($\sim 1000 \text{ cm}^2/\text{V.s}$) and GaN ($\sim 1200 \text{ cm}^2/\text{V.s}$). Moreover, the electron mobility of $\beta\text{-Ga}_2\text{O}_3$ ($\mu_{\text{experiment}} = 20\text{--}170 \text{ cm}^2/\text{V.s}$) is much lower than the theoretical expectation ($\mu_{\text{theory}} = 300 \text{ cm}^2/\text{V.s}$) in the experiment [15].

On the one hand, the low mobility is due to a large number of defects inside $\beta\text{-Ga}_2\text{O}_3$. Therefore, the modulations of defects are very urgent and vital to realizing high performance of $\beta\text{-Ga}_2\text{O}_3$ based devices. On the other hand, the reasons are attributed to the

different scattering mechanisms of electrons within different temperature ranges and the complex vibration modes of phonons in $\beta\text{-Ga}_2\text{O}_3$ [15]. Figure below presents the variation of electron mobility with temperature.

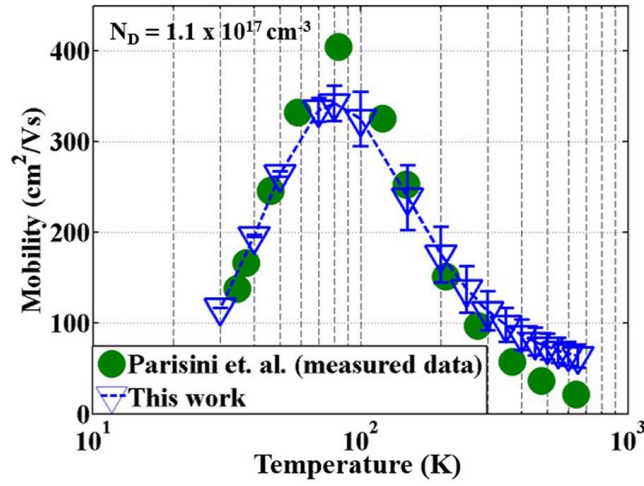


Figure I.12: Variation of electron mobility in $\beta\text{-Ga}_2\text{O}_3$ with temperature[51].

From the figure we observed that despite this increase in the carrier concentrations, the mobility decreases due to the free carriers collide with the impurities more frequently (**figure I.13**), so the drift velocity decreases [52].

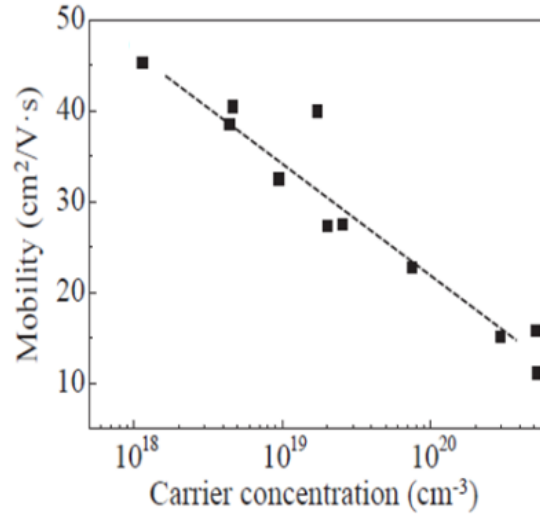


Figure I.13: Relationship between mobility and carrier concentration for Sn-doped $\beta\text{-Ga}_2\text{O}_3$ films[53].

I.5.5.3.Free electron concentration and resistivity:

The free concentration of carriers, such as electrons and holes, in $\beta\text{-Ga}_2\text{O}_3$ plays a critical role in determining the electrical and optical properties of the material. Intrinsic carrier concentration of $\beta\text{-Ga}_2\text{O}_3$ is in very low [54]. This is due to a number of reasons, including:

✓Doping:

Through Hall effect measurements on samples from un-doped $\beta\text{-Ga}_2\text{O}_3$ we noticed that the carrier concentration is low, and the crystal shows a semi-insulating property [51]. In order to enhance its electrical properties, we can be artificially introducing doping elements [55]. The two most common n-type dopants $\beta\text{-Ga}_2\text{O}_3$ are group IV element such as Si, Sn[52]. The carrier concentrations in Si- and Sn-doped crystals are very high as we shown in the table below[51].

Table I.2: Electric properties measured by Hall effect measurement [51].

	$n(\text{cm}^{-3})$	$\mu(\text{cm}^2/\text{V s})$	$\rho(\Omega.\text{cm})$
Un-doped	3.1×10^8	33	8.8×10^8
Si-doped	3.0×10^{18}	80	2.6×10^{-2}
Sn-doped	2.2×10^{18}	72	3.9×10^{-2}

However, the selection of dopant elements and concentration can also impact the free carrier concentration and overall electronic behavior of the material for example it is difficult to achieve a high doping concentration with Si as a dopant, usually not over 0.2 mol%. On the other hand, SnO_2 and Ge evaporate easily at high temperature, so it is not easy to obtain a high doping concentration Sn/Ge doped $\beta\text{-Ga}_2\text{O}_3$ single crystals by melt methods [52].

✓ Defects:

The presence of defects can affect its electrical properties, including free carrier concentration. These defects can create energy states within the bandgap that can trap or release carriers, thus altering their concentration and mobility, such as oxygen vacancies that act as deep donors, which cannot directly contribute to the electrical conductivity [27],[18].

✓ Crystal growth:

The method and conditions of crystal growth can impact the free carrier concentration in beta gallium oxide as the free electron concentration could be controlled by growth conditions, post-growth treatment, or intentional doping [20]

The decrease of resistivity can be explained by the presence of the Sn^{+4} ion. When some of the Ga^{+3} ions in the lattice are replaced by Sn^{+4} or some of the Sn ions as interstitial atoms are located in the lattice, conduction electrons can be produced, thus the resistivity of films is reduced. However, as Sn concentration increases further (over 10%), the crystalline quality of the films becomes poor. Consequently, the defects inside the films lead to the enhancement of the carrier scattering effect, and also the doping efficiency drops[56].

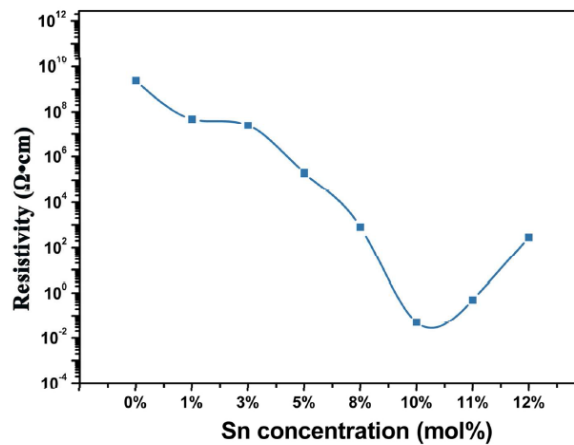


Figure I.14: The resistivity of the $\beta\text{-Ga}_2\text{O}_3$ films with different Sn concentrations[56].

I.5.5.4. Breakdown electrical field:

The large breakdown voltage, is especially interesting for devices in power electronics, where the ability of devices to handle high power densities is sought after [32]. The breakdown electric field (E_{br}) is an intrinsic property that each material has and corresponds to the maximum electric field that the material structure can support before breakdown [45],[57]. When an electric field is applied, electrons gain energy from the electric field and cross the forbidden energy gap from the valence band to the conduction band. When this process is repeated, more and more electrons become available in the conduction band, eventually leading to breakdown [58].

The breakdown field of $\beta\text{-Ga}_2\text{O}_3$ is estimated to be in the range of 8 MV/cm[59], which is very much higher than others, like GaN (~5 MV/cm) and SiC (~3 MV/cm)[29], as can be seen in **figure I.15** opens the scope for high voltage and high temperature applications[7].

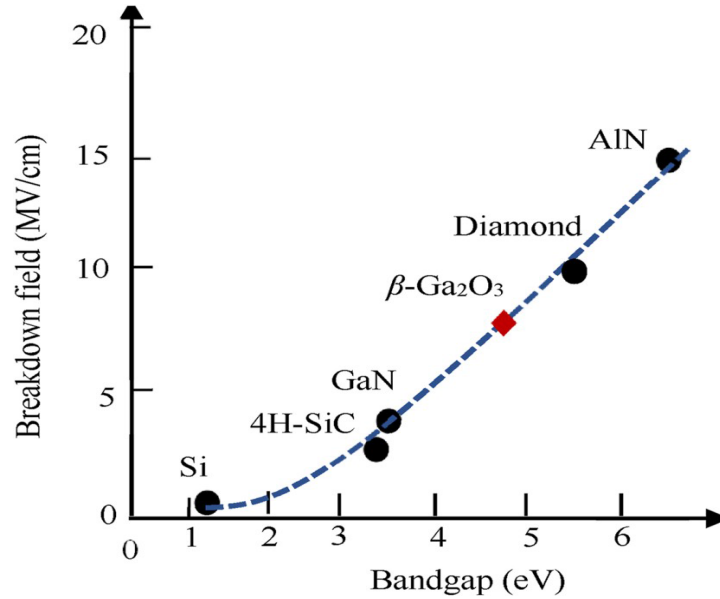


Figure I.15: Electric breakdown fields corresponding to bandgap of major WBG semiconductor material[60],[61].

The higher electric breakdown field enable greater voltage blocking capability, high temperature operation, and allows deeper doping concentration. Therefore, it results in lower conduction losses and a low resistance. Thus, it results an on-resistant reduction in comparison with Si-based devices[62]. In addition, The large bandgap of $\beta\text{-Ga}_2\text{O}_3$ allows it to withstand a stronger electric field, which makes it possible to use a thinner device for a given voltage rating[63]. These lead to much faster switching behaviour [64]. There is also the low cost of production due to the ability to grow large melt grown crystals [65].

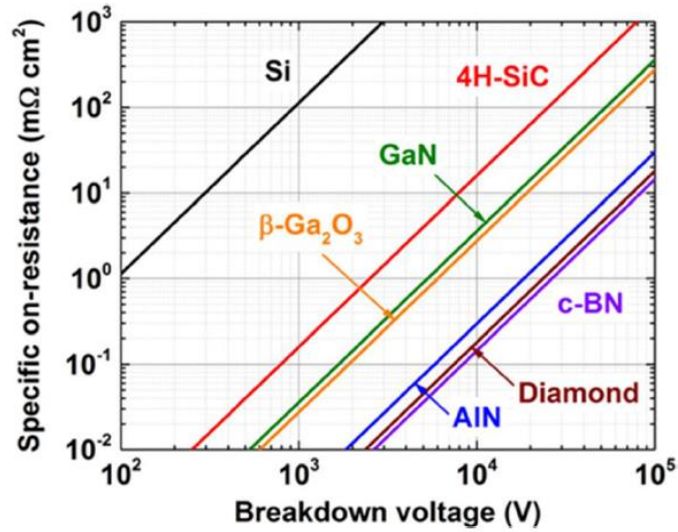


Figure I.16: Comparison of breakdown voltage and specific on-state resistance in candidate materials for high power electronics [66],[18].

As a result, $\beta\text{-Ga}_2\text{O}_3$ based devices are promising candidates for efficient power conversion application in smart grids, renewable energy, big data center power supplies, and automotive electronics [63]. Currently non-accessible with SiC and GaN, if not capable to replace them fully [46].

I.5.6 Optical properties:

As a promising material for optoelectronic devices, the understanding of optical properties of $\beta\text{-Ga}_2\text{O}_3$ is very necessary [67]. The basic optical properties of $\beta\text{-Ga}_2\text{O}_3$ stems from the crystal structure and electronic band of the material [68]. Here are some of the key optical properties of $\beta\text{-Ga}_2\text{O}_3$:

I.5.6.1. Optical bandgap:

Band gap defines one of the most important optical properties of beta gallium oxide [29]. It has a wide band gap ~ 4.8 , which is intrinsically suitable for fabricating solar-blind ultraviolet photodetectors. Owing to its wide band gap, pure $\beta\text{-Ga}_2\text{O}_3$ crystals are colorless

and extremely transparent from UV to near-infrared (NIR) spectra of the light spectrum [37],[68]. However, colouration of the crystals can be caused by impurities or specific growth conditions. for instance, as we mention above Insulating $\beta\text{-Ga}_2\text{O}_3$ crystals (pure $\beta\text{-Ga}_2\text{O}_3$) are either colourless or had a light yellowish colouration; which was caused by some minor absorption in the blue part of the visible spectrum. Also in case of Conductive n-type crystals had bluish colouration; which was caused by increased free carrier absorption in the red and NIR regions of the spectrum. Additionally, there is the greyish colouration, which is caused by impurities e.g. carbon[17].



Figure I.17: Some examples of coloration of $\beta\text{-Ga}_2\text{O}_3$ crystals[33].

I.5.6.2. Reflection index:

The refractive index of $\beta\text{-Ga}_2\text{O}_3$ typically is around 1.95 and 2.1 [43] depending on the wavelength and crystal orientation [18]. With a high anisotropy just near the absorption edge in the UV region[43].

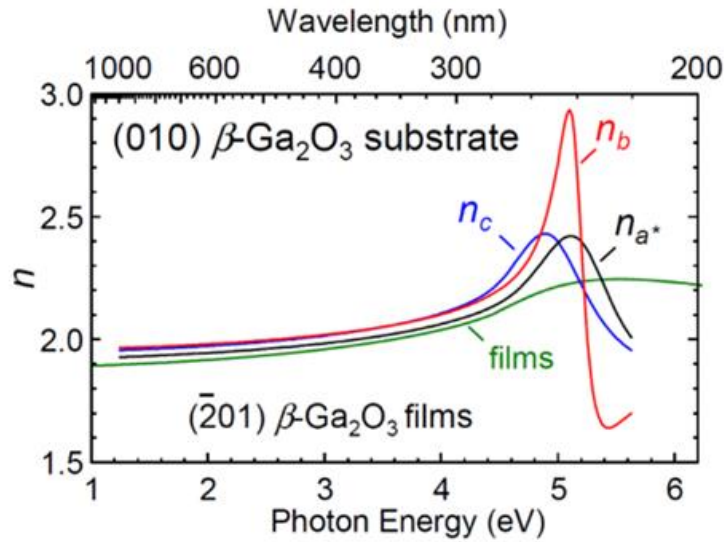


Figure I.18: Spectra for refractive index n of $\beta\text{-Ga}_2\text{O}_3$ thin film and substrate [68].

I.5.6.3. Transmission and absorption:

As an ultrawide bandgap semiconductor, $\beta\text{-Ga}_2\text{O}_3$ has high transmittance and low absorption in the visible and near infrared regions of the solar spectrum, so it can be applied in transparent conductive electrodes in some areas [15]. **Figure I.19** is shown the transmittance spectra of $\beta\text{-Ga}_2\text{O}_3$ crystals.

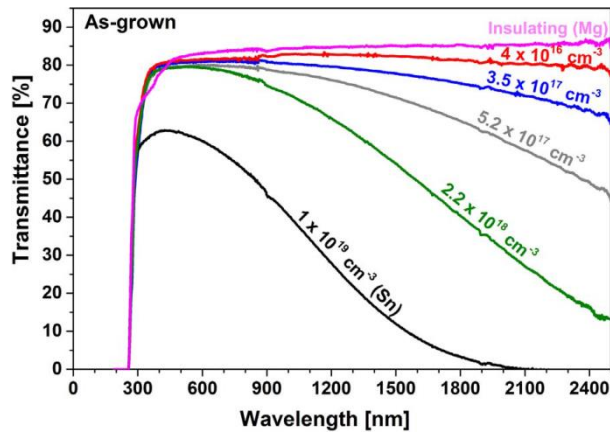


Figure I.19: The transmittance spectra of $\beta\text{-Ga}_2\text{O}_3$ crystals [69].

From this figure we can notice that:

- ✓The $\beta\text{-Ga}_2\text{O}_3$ crystals has a high transmittance between 80% and 85% from the UV to infrared (IR) wavelength region [43].
- ✓This figure shows an absorption peak which are located in the ultraviolet region, and it has strong absorption in the solar-blind ultraviolet region [15], and a good transparency in the visible and near infrared (NIR) spectra at low electron concentrations[69].
- ✓The transmittance deteriorates with increasing free electron concentration due to free carrier absorption, especially in the red and NIR spectra. This effect is pronounced at free electron concentrations above 10^{18}cm^{-3} . At low concentrations, the crystals are substantially fully transparent in the visible and ultraviolet (UV) spectrum, making this compound suitable for optoelectronic applications in these parts of the electromagnetic spectrum [69].

The **figure I.20** is shown the absorption spectra of $\beta\text{-Ga}_2\text{O}_3$, we can notice that there is a steep cutoff absorption edge at approximately 255~260 nm with a shoulder approximately 270~275 nm[37]. The absorption edge at 255~260 nm was due to the intrinsic band-to-band transition while the absorption at 270~275 nm was caused by Ga^{3+} vacancies in the conduction band [35].

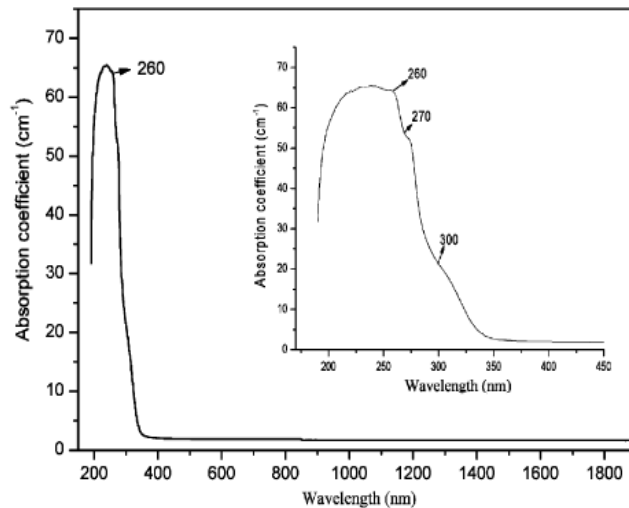


Figure I.20: The absorption spectra of $\beta\text{-Ga}_2\text{O}_3$ single crystal [70].

Therefore, the sample of the $\beta\text{-Ga}_2\text{O}_3$ has a good optical properties for potential applications to solar-blind (220 nm–280 nm) detectors [71].

I.5.7 Thermal properties:

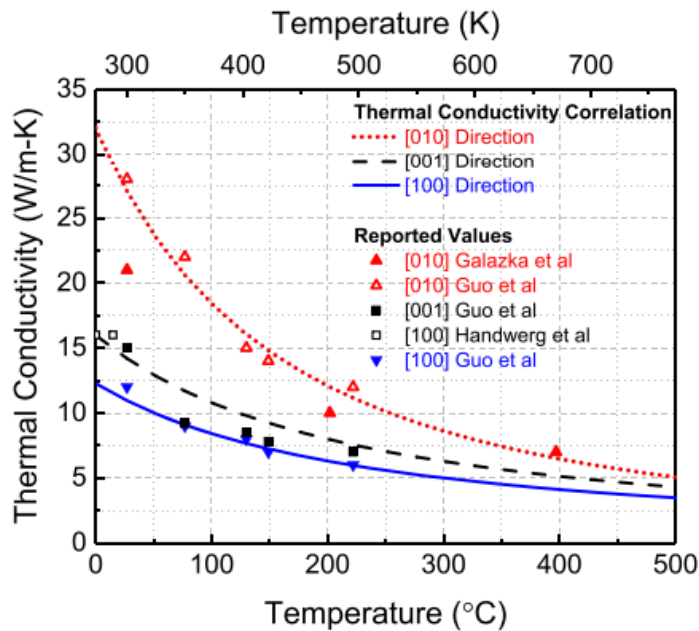
Thermal properties of $\beta\text{-Ga}_2\text{O}_3$, which are summarized in **Table I.3** [69]

Table I.3: Thermal properties of $\beta\text{-Ga}_2\text{O}_3$ [69].

Axis	Thermal diffusivity mm^2/s (RT)	Thermal conductivity $\text{W}/\text{m}\cdot\text{K}$ (RT)	Thermal expansion $10^{-6}\times\text{K}^{-1}$ (650 K)
a [100]	3.7	11	4.7
c [001]	7.1	21	8.5
b [010]	9.6	29	8.3

The thermal conductivity is one of the important parameters to make a great impact on performance of high power devices, since it limits dissipation capacity of heat generated by on-state conduction loss in the channel and/or drift regions $\beta\text{-Ga}_2\text{O}_3$ has a significantly lower thermal conductivity compared to those of the other power (Si (130 W/mK), GaN (150-200 W/mK), and SiC (360-490 W/mK) [72],[45].

As we noted from the **table I.3**, the thermal conductivity in $\beta\text{-Ga}_2\text{O}_3$ shows a strong anisotropy; and that due to the monoclinic lattice structure. They were estimated to be ~ 29 W/mK in the [010] direction (highest) and ~ 11 W/m.K in the [100] direction (lowest) [45]. This low thermal conductivity is undesirable in high voltage devices based on $\beta\text{-Ga}_2\text{O}_3$ [73]. The other disadvantage is that the thermal conductivity falls rapidly with temperature, so



that high temperature device operation is particularly problematic with $\beta\text{-Ga}_2\text{O}_3$ [74].

Figure I.21: Temperature dependence of the thermal conductivity of $\beta\text{-Ga}_2\text{O}_3$ in different crystallographic directions.

The low thermal conductivity will not only hamper high-power device performance but also limit long-term device reliability. Hence, thermal management is one of the key technical challenges for future practical applications and industrialization of devices based on $\beta\text{-Ga}_2\text{O}_3$ [45].

CHAPTER II:
Background of β -Ga₂O₃
solar blind photodetectors

II.1- Introduction :

Photodetection in the ultraviolet (UV) region has drawn extensive attention owing to its various applications in industry and our daily life including ozone holes monitoring, geological exploration, short-distance communication, missile early warning and tracking, chemical and pharmaceutical analysis, inspection of UV leakage[3],[75].

The ultraviolet (UV) radiation, a part of the solar radiation (10-400 nm)[3]. It is typically divided into four spectral regions: UV-A (for wavelengths between 400 and 320 nm), UV-B (for wavelengths between 320 and 280 nm), UV-C (for wavelengths between 280 and 200 nm), and far UV (for wavelength between 200 and 10 nm). Most of the UV light from the Sun, it is absorbed by the atmospheric ozone layer[75]. Due to this absorption, there are less ultraviolet radiation with wavelengths of 220 ~ 280 nm surface of the earth, this range of solar radiation named the solar-blind ultraviolet regime. Thus, solar-blind UV photodetectors have the high-precision detection and strong anti-interference ability, even exposed to sunlight[3].

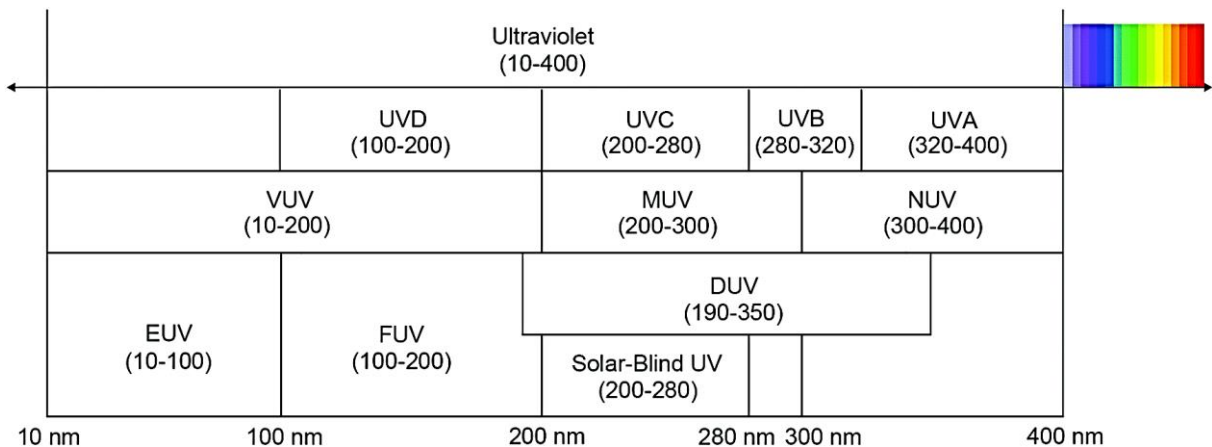


Figure II.1: Subdivision diagram of the ultraviolet light region[76].

Unfortunately, the commercially available solar-blind photodetectors are usually photomultiplier tubes which are bulky, fragile, and require the large bias voltage, thus limiting their applications[77]. So with the rapidly increasing demand for solar-blind ultraviolet (UV) photodetectors (PDs), several research groups have studied the development of novel wide-bandgap materials that guarantee to us a strong radiation hardness, high thermal and chemical stability, making them feasible to be applied in harsh environment[78]. β -Ga₂O₃ is considered as one of the most promising candidates for solar-blind detection because of his unique properties (having a wide bandgap of \sim 4.8 eV, good chemical and thermal stability, high optical transparency in both UV and visible regions, low cost[79] and the intrinsic radiation hardness of the material allows its usage in extremely harsh environments such as space exploration[80])[81], [82]. All these features facilitate β -Ga₂O₃ to become the optimal material for the fabrication of solar-blind ultraviolet photodetectors[83]. Nowadays, great efforts have been made to fabricate self-powered devices based on β -Ga₂O₃, that can work in the absence of external power supply, which are suitable for application in unmanned hazardous atmosphere or harsh environment. Self-powered photodetectors can be realized by photovoltaic effect by means of Schottky junctions, p-n junctions and heterojunctions[77].

In this chapter, we will explore the different types of solar-blind UV photodetectors based on β -Ga₂O₃ and traced their development and we will focus on those devices based on Schottky junction.

II.2- Background and motivation of studying solar blind photodetector based on beta gallium oxide:

Traditionally, solar blind photodetectors were fabricated using mature technology such as silicon. However, the devices based on this technology have an unwanted broadband spectral response due to the bandgap of 1.1 eV. To overcome this, use of optical filters (such as Wood's filters) became necessary. These filters work by transmitting UV light while blocking or removing the visible part of the solar spectrum. Such filters are not just costly

(thereby increasing the cost of the device) but also have the issue of “solarization,” i.e. as a result of repeated use, the device starts to emit visible light leaks, thus decreasing the lifetime of the device. In addition, filters such as those based on dielectric interference films or metal-dielectric based filters have low transmittance in the UV region. This gave an impetus to look for newer materials free from these constraints and the answer lay in materials with a bandgap much greater than that of silicon i.e. “wide band gap materials”.

Wide bandgap materials are those that have a bandgap that is greater than that of conventional semiconductors (3 eV) and lower than that of insulators (7 eV). Using these, it is possible to create photodetectors that are sensitive to the entire UV spectrum, eliminating the need for optical filters and the solarization issue. Materials such as 4H-SiC (E_g = 3.2 eV), ZnO (E_g = 3.37 eV), GaN (E_g = 3.4 eV), AlGa₂N (E_g = 3.4–6.2 eV), Ga₂O₃ (E_g = 4.6–5.3 eV), diamond (E_g = 5.5 eV) all classify as WBG and hence are often used as absorber materials. Most of these have different forms and polytypes which make their bandgap spread to a range of values. For the special case of solar blind photodetector, corresponding to a wavelength of less than 280 nm, the bandgap required has to be greater than 4.4 eV. This prerequisite disqualifies some of the WBG materials, leaving behind a few worthy candidates, the so called ultrawide bandgap (UWBG) materials. Among these, beta gallium oxide is one of the more suitable materials that can be used to model and fabricate these solar blind photodetectors [80].

In 2008, solar-blind UV photodetectors based on Ga₂O₃ single crystal substrates were initially developed since that, Ga₂O₃ solar-blind UV photodetectors have been broadly studied in the types of metal-semiconductor-metal (MSM) photodetectors, Schottky barrier photodetectors, and p-n,p-i-n junction photodiodes [84]. The recent developments in high beta gallium oxide material growth technology made it possible to fabricate high performance solar-blind photodetectors operating in the ultraviolet (UV) spectral region with improved receiver sensitivity, low noise, low dark current density, and high speed [85].

II.3- Operating principle of Photodetector:

Photodetector is specialized device that is designed to detect specific range radiation even while exposed to sunlight through convert light energy into an electrical one [80], primarily as current or voltage[86]. Regardless of the photodetector architecture, the basic principal of operation of all photodetectors is the same[87] and it includes basically three processes: 1) generation of photogenerated carriers by incident light, 2) the transport of photogenerated carriers along with any multiplication by the current-gain mechanism (if present), and 3) charge carrier extraction at the end electrode to provide the output signal[80].

II.4- Basic Parameters of UV photodetectors:

After a long-time exploration of photodetectors, researchers have developed a mature system of detector evaluation indicators[76].

II.4.1 Dark current:

Dark current refers to the tiny current that is still generated on a device when no photons pass through photodetectors (such as photomultipliers, photodiodes, and charge-coupled devices)[76].

II.4.2 Responsivity:

The responsivity is one of the basic parameters to evaluate the sensitivity of a photodetector[1]. It represents the ability of a detector to convert an optical signal to electrical signal[86]. We can defined it as the ratio of generated photocurrent and incident optical power, and is determined by the following Equation [80], [39]:

$$R = \frac{I_{ph}}{PS} = \frac{I_{light} - I_{dark}}{PS} \quad (II.1)$$

where I_{ph} is the photocurrent at incident illumination, I_{dark} is the current in the dark condition, P is the light power density, and S is the effective illuminated area, . Usually measured in Ampere per Watt (A/W).

The photocurrent refers to the electric current generated by the photodetector; when a photon with sufficient energy strikes the photodetector; this will generate an electron–hole pair; if the absorption of photons occurs in the depletion layer, the internal electric field in this region will eliminate the barrier between the electrons and holes such that holes can move towards the anode and electrons can move towards the cathode; therefore, the photocurrent is generated [76].

the measured photocurrent is a combination of dark current and light-generated current, which also shows that the dark current must be minimized to improve the sensitivity of devices towards the light [76].

II.4.3 Response time:

The response speed is normally described by the response time of the photodetector[1] because When photons are irradiated on photodetectors, these devices do not change instantaneously with changes in external conditions because carrier migration takes time. This transit time is the response time[76].It is usually measured in two separate components: rise time (τ_r) and decay time (τ_d)[80]. The rise time can be defined as the time required for the photocurrent of devices to increase from 10% to 90% of the maximum value; similarly, the decay time can be defined as the time to reduce the photocurrent of devices from 90% of the highest value to 10%[76]. It is measured in seconds[80].

II.4.4 Specific detectivity (D^*):

The specific detectivity (D^*) represents the ability to differentiate the smallest light intensity from noise. It is defined as [39],[88]:

$$D^* = \sqrt{\frac{A_{op}}{2qI_{dark}}} R \quad (II.2)$$

where A_{op} is the effective area under illumination, I_{dark} is the dark current, R is the responsivity, q is electron charge.

II.4.5 Quantum efficiency :

The ability of the photodetector to convert the input light to an output electrical signal is called quantum efficiency [80]. It is typically defined as the percentage of photons received on the light-receiving surface that are converted into electron-hole pairs. Quantum efficiency is divided into external quantum efficiency (EQE) , and internal quantum efficiency(IQE)[76]. Internal quantum efficiency (IQE) is defined as ratio of the number of electron-hole pairs generated in the semiconductor to the number of incident photons per second whereas external quantum efficiency (EQE) represents the ratio of the number of electron-hole pairs collected (contributing to the photocurrent) to the number of incident photons per second. Both IQE and EQE are measured in terms of percentages. Usually, EQE is the preferred figure-of-merit in gallium oxide based photodetectors and is determined by the following equation [39]Ⓜ:

$$\mathbf{EQE} = \frac{I_{ph}/q}{(PS)/h\nu} = \mathbf{R} \frac{h\nu}{q} \quad (\text{II.3})$$

Where I_{ph} is the photocurrent, q is electron charge, P is the light power density, S is the effective illuminated area, h is Planck's constant ν is frequency of incident light, , R is the responsivity.

II.4.6 Gain:

The number of photogenerated carriers collected by the electrodes divided by the absorbed photons[78]. It defined as [76]Ⓜ:

$$\mathbf{g} = \mathbf{log}_{10}(P_{out}/P_{in}) \quad (\text{II.4})$$

where P_{out} is the power of output signals, and P_{in} is the power of input signals.

II.4.7 Linear dynamic range:

Linearity of a Photodetector implies the linear response of the device to input optical power. That is, the output electrical signal (i.e., the photocurrent), should vary linearly with

the power of the optical signal incident on the device. Linear response results in reliable device operation in the sense that it enables a distortion-free and faithful conversion of optical signal to electrical signal. Linearity ensures that the responsivity is constant and independent of the incident power intensity. This linearity arises from the fact that for low light intensity, the concentration of excess carriers (i.e., photocarriers) generated is linearly proportional to the optical generation rate and hence to the input optical power. However, beyond a certain optical power, the output photocurrent no longer scales linearly but tends to saturate and deviate from linearity. It may be noted that in the presence of traps and/or recombination centers, more complicated, nonlinear dependence of photocurrent on optical power level may arise[86]. The dynamic range of a photodetector is defined as [78]:

$$\text{LDR} = 20 \log(I_{\text{ph}}/I_{\text{dark}}) \quad (\text{II.5})$$

Where I_{ph} and I_{dark} are photocurrent and dark current, respectively.

II.5- β -Ga₂O₃ solar-blind UV photodetectors :

There are several types of semiconductor device architectures that can be used to create photodetectors including photoconductor, metal semiconductor metal (MSM), Schottky, p-n, and pin junction [87].

II.5.1-Photoconductors:

One of the most common device architectures for solar blind detection is a photoconductor that is structurally defined by a semiconductor layer as a channel with two Ohmic contacts affixed to opposite ends of the channel. The working principle relies on the process in which photon absorption by the semiconductor produces excess free carriers and gives an increase in conductivity. Under illumination, the semiconductor can absorb photons with energy higher than its bandgap, which generates electron-hole pairs. The electron-hole pairs are then separated by the applied voltage, and the free electrons and holes drift oppositely toward electrodes[89]. The change in the amount of these carriers ends up being the output signal in the form of an increased current called photocurrent . the role of use

The Ohmic contacts (mostly metal) is To facilitate the transfer of charge carriers across the device and into the external circuitry; because The Ohmic contact poses no barrier to the replenishment of electrons into the semiconductor [80].

These devices offer the benefits of a simple fabrication, low cost, They often have a high gain, large photoresponsivity, but slow response time and lack of a need for amplifying equipment , in addition, they are not difficult to integrate them with other devices on a chip. however, they also have a higher dark current along with higher associated noise, the photoconductor has strong persistent photoconductivity, meaning that photocurrent persists even after removal of illumination . In addition, it is not possible for a photoconductor to operate at zero bias, meaning that it consumes more power. Photoconductors also exhibit poor contrast between UV and visible light[35], [80].

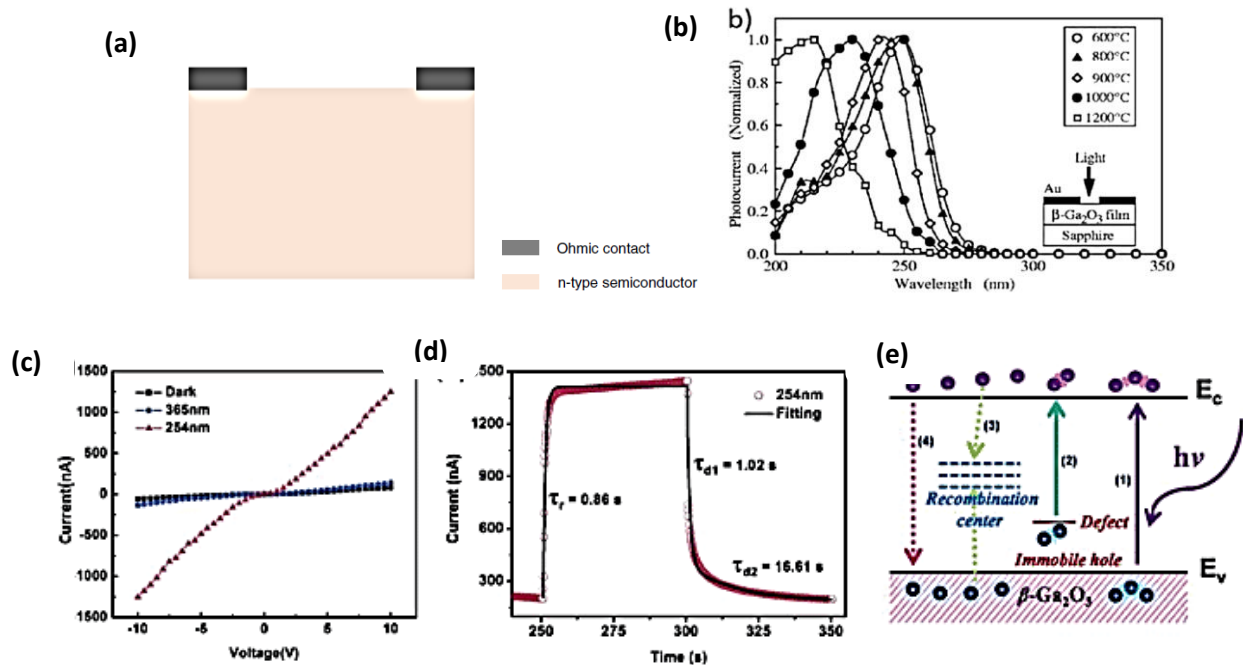


Figure II.2: (a) Schematic structure of a photoconductor[1]. (b) Spectral responses of the photoconductors based on β -Ga₂O₃ films prepared at various temperatures. (c) Current-voltage (I - V) characteristics of the β -Ga₂O₃ photodetector in dark, under 365 and 254 nm light radiation. (d) Experimental curve and fitted curve of the current rise and decay process to 254 nm illuminations. (e) Schematic diagram illustrating the carrier transport mechanism in the β -Ga₂O₃ photodetector[89].

II.5.2- MSM photodiode:

MSM (metal–semiconductor–metal) photodiodes are a commonly used structure for β -Ga₂O₃ photodetectors. Usually, a MSM photodetector is composed of two back-to-back Schottky by depositing interdigitated metal electrodes on the surface of the active layer. A schematic of MSM photodetector structure is shown in **figure II.3**. A MSM photodiode has fast operation due to a low capacitance per unit area. The device also has a simple structure that is easy to fabricate and integrate. However, there is intrinsic low responsivity due to the interdigitated electrodes covering the active region. MSM photodiodes have high gain and are easy to integrate with read-out circuitry. The interdigitated electrodes need to be close together to maintain device performance, but this lowers responsivity because it blocks part of the incoming light. , and the reflection of light from surface metals is a problem. There is good contrast between the visible and the UV spectrum, and the bandwidth is wide. However, noise is a significant problem and the material has high resistivity [35].

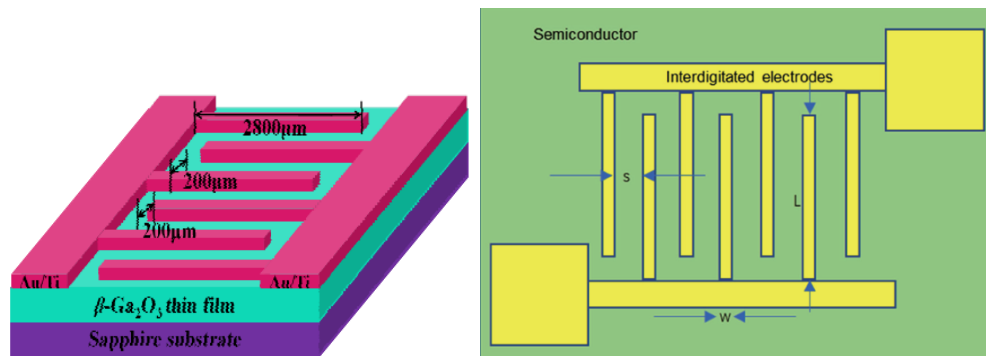


Figure II.3 :Schematic structure of MSM photodetector [78].

II.5.3-PN photodiode:

A p-n photodiode is a p-n diode made with materials that allow light to penetrate the p-n junction. It has a fast response speed and low dark current, and can operate without an

applied bias, so it consumes less power. The photoresponse is linear with optical power. For β -Ga₂O₃ devices, there is good rejection of light from the visible spectrum. The time response is limited by p-doping[35].

P-N photodetectors are normally geometrically composed of junctions with opposite doping types. The working mechanism relies essentially on the photovoltaic effect: due to the difference in work functions, charge transfer takes place between two semiconductors until their Fermi levels align. In the meantime, a region of free charges is depleted near the interface and a built-in electric field is created. As a result, an energy barrier preventing the flow of charge carriers across the junction is formed because of the discontinuity in allowed energy states of the two semiconductors at equilibrium state. Upon illumination, photons with energy higher than the bandgap are absorbed by the semiconductors, which creates electron-hole pairs in the material on both sides of the junction. The electrons and holes generated within a diffusion length from the junction travel to the space charge region, where they are separated by the built-in electric field and then propelled toward opposite directions.. The p-n photodiodes can operate at two modes: 1) photovoltaic (operation at zero bias) and 2) photoconductive (operation under reverse bias). At the first mode, a photodiode usually has an improved specific detectivity (D^*) and maximum linearity and sensitivity due to relatively low dark current. Under reverse bias, the depletion region will be widened and the photodiode can have a faster response speed thanks to the reduced transit time and lowered diode capacitance [89].

As an intrinsic n-type semiconductor, β -Ga₂O₃ is difficult to realize p-type doping, thus few reports on β -Ga₂O₃ homojunction devices can be found. Therefore, heterojunction devices turn out to be an alternative to construct β -Ga₂O₃ based photodetectors. To date, β -Ga₂O₃ heterojunctions based on SiC, SnO₂ and ZnO have been reported to construct solar-blind photodetectors[77].

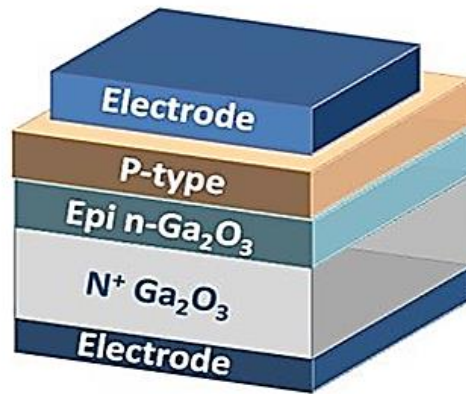


Figure II.4: Schematic structure of p-n heterojunction diode [90].

II.5.4-P-I-N photodiode:

P-I-N photodiodes are similar to p-n photodiodes, except for the addition of an intrinsic layer between the p and n materials. In a p-i-n junction photodiode, absorbed photons generate electron-hole pairs, which are collected by the n and p layers due to the reverse bias. Carriers generated in the junction experience a high electric field and are separated rapidly, giving the detector a fast response. The addition of an intrinsic layer improves absorption and increases the quantum efficiency. To reduce the capacitance, the thickness of the intrinsic layer can be increased. However, a thicker intrinsic layer increases the transit time. The junctions are critical to device performance, because if recombination occurs in the junctions, device performance is degraded. There is a good UV-to-visible rejection ratio, sharp spectral responsivity cutoff, and fast response time [35].

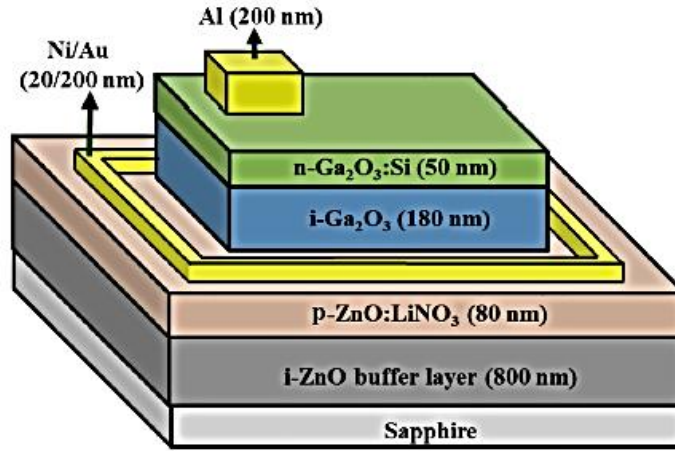


Figure II.5: Schematic structure of an example of solar blind photodiode based on pin photodiode: solar blind p-ZnO:LiNO₃/i-Ga₂O₃/n-Ga₂O₃:Si [91].

II.5.5-Schottky photodiode

Due to a paucity of bipolar devices owing to no reliable and stable p-type doping of β -Ga₂O₃ have been achieved [13], and the complexity of heterojunction, one needs to look for other ways to achieve an effective separation of charge carriers. This can be done with the use of the concept of a Schottky barrier[80]. Schottky barrier photodiodes have been extensively studied and used as UV detectors., these devices show advantages including : operate without external power sources owing to the photovoltaic effect, simple and low-cost fabrication, no high-temperature diffusion process , high quantum efficiency, low dark current, and high UV/dark current ratio because of the existence of Schottky barrier, high-speed response and high photosensitivity [76], [78], [84]. Thus most of β -Ga₂O₃ based photodetectors are of Schottky type structures [13].

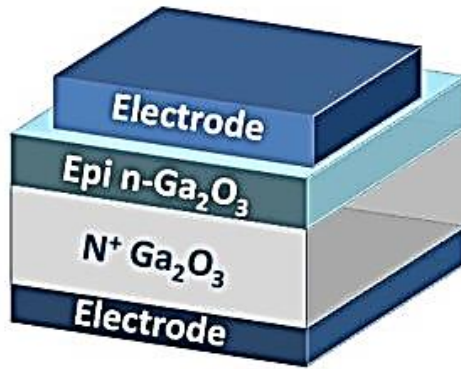


Figure II.6 : Schematic structure of schottky diode

Besides great advantages and progresses mentioned above, there are still several drawbacks on Schottky-type UV photodetector. Firstly, the depth of depletion layer in Schottky junction is relatively shallow. This will restrict the effective separation of e-h pairs. Secondly, Schottky barrier is serious affected by the surface state of semiconductor, which requires precisely control of the interface between metal and semiconductor. Therefore, efforts and attentions need to be paid to strengthen the barrier height and the stability of the Schottky junction[84].

II.6- The basic Concept of Schottky Barrier Diode:

The simplest schottky photodiode is basically made up of a metal layer in contact with a semiconductor whose work function is quite different from that of a metal[89]. When a contact between a suitable metal with work function Φ_M is established with the intrinsically n-type gallium oxide having a different work function Φ_S ($\Phi_M > \Phi_S$) electrons transfer from the semiconductor to the metal. This leads to a bending of the electronic bands (to reach the equilibrium) leading to the development of a Schottky barrier height at the interface. This forms a built-in potential (a sort of depletion region) that effectively separates the charge carriers [80], [92].

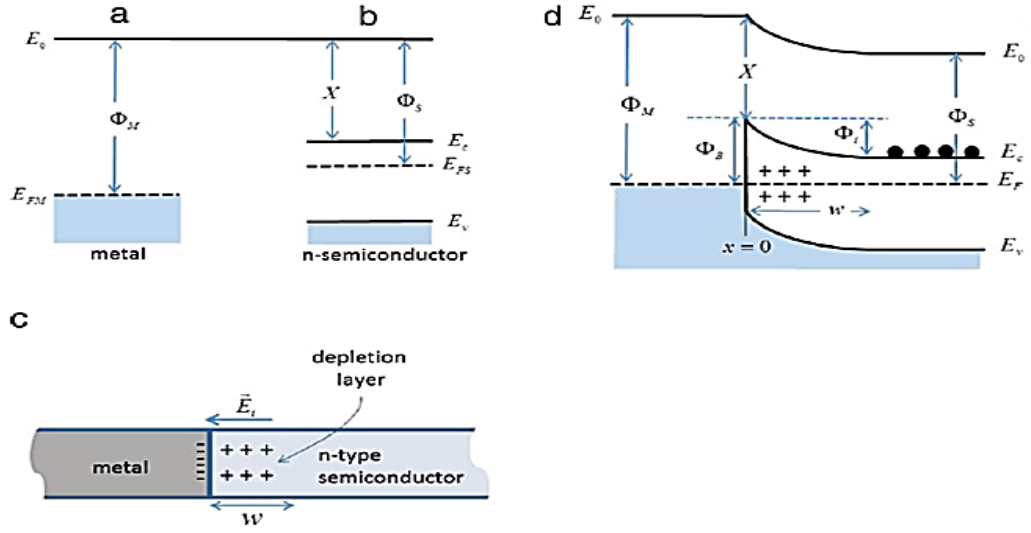


Figure II.7 : A Schottky barrier formed by a metal of high work function contacting a n-type semiconductor. **(a)** Metal work function Φ_M and Fermi energy E_{fM} . **(b)** Semiconductor work function Φ_S , electron affinity χ and band structure with a bandgap between E_c and E_v and Fermi energy E_{fS} . **(c)** Charge at the metal/semiconductor junction. **(d)** Idealized equilibrium band diagram for the metal/semiconductor junction. The physical junction is set at $x = 0$. Φ_i is the energy barrier to the flow of electrons (black dots) from the semiconductor to the metal, while Φ_B is the Schottky barrier height (SBH) for the electron flow in the opposite direction. w is the extension of the depletion layer and corresponds to the bent part of the energy bands[23].

With reference to **figure II.7**, the vacuum level E_0 (or the free-electron energy), which is a convenient reference level for energy, is the energy state of electrons with zero kinetic energy outside the material, either metal or semiconductor. E_0 , as all other energies in this context, is expressed in eV. The difference between E_0 and the Fermi level E_f in any material is called the work function Φ

$$\Phi = E_0 - E_f \quad (\text{II.6})$$

The Fermi energy E_f represents the highest occupied electron energy state at $T = 0$ K in a metal. In a non-degenerate semiconductor it lies in the gap between the valence and the

conduction band, and, as in metals, it separates the occupied from the unoccupied states at $T = 0$ K. E_F is the parameter that appears in the Fermi–Dirac distribution function.

$$f(\mathbf{E}) = \frac{1}{1 + e^{(E - E_F)/KT}} \quad (\text{II.7})$$

which expresses the probability that an electron occupies a state with energy E at the absolute temperature T ($k = 8.62 \times 10^{-5}$ eV/K is the Boltzmann constant). According to this Equation, for $T > 0$ K, electrons can occupy levels above the Fermi level with a rapidly decreasing probability as the energy moves away from E_f . For metals, the work function $\Phi_M = E_0 - E_{fM}$ is the energy required to remove an electron at the Fermi level E_{fM} to the vacuum and has a value which depends only on the type of metal (metal workfunctions are comprised between ~ 2 and 6 eV). In a semiconductor, the position of E_{fS} depends on the doping: E_{fS} is closer to E_c (the lowest allowed energy level of the conduction band) for a n-type semiconductor. The electron and hole densities in a semiconductor, denoted by n and p respectively, are in fact related to the Fermi energy by the relations :

$$\mathbf{n} = N_c e^{-(E_c - E_f)/KT} \quad (\text{II.8})$$

and

$$\mathbf{p} = N_v e^{-(E_f - E_v)/KT} \quad (\text{II.9})$$

Where $N_c = 2(2\pi m_e^* KT/h)^{3/2}$ and $N_v = 2(2\pi m_t^* KT/h)^{3/2}$ are the effective densities of states in the conduction and valence band, and m_e^* and m_t^* are the effective masses of electrons and holes, respectively ($h = 4.136 \times 10^{-15}$ eV.s is the Planck constant).

Since the Fermi level is not fixed, the work function in a semiconductor varies according to the doping and is not a good parameter to consider. A constant quantity that, alike Φ_M , can be used to characterize a semiconductor material is rather the difference between the vacuum level and the conduction band edge, known as the electron affinity and is denoted as χ :

$$\chi = E_0 - E_c \quad (\text{II.10})$$

When a depletion layer is formed in the semiconductor, the space charge is mirrored by a very thin layer of opposite-sign charge at the metal surface (**Figure II.7(c)**). These two layers of opposite charge give rise to an electric field which prevent further net charge diffusion between the semiconductor and the metal. Φ_i is called the energy barrier against the diffusion of electrons from the semiconductor to the metal, is obtained as

$$\Phi_i = \Phi_M - \Phi_s \quad (\text{II.11})$$

The electric field E is oriented from the positive charge of the depletion layer of the n-type semiconductor towards the negative charge at the metal surface, is the built-in electric field and opposes to the motion of electrons from the semiconductor to the metal. It has the maximum value at the physical metal semiconductor interface ($x = 0$) and decreases with distance until it vanishes at the edge of the depletion layer (i.e. at $x = w$). The most important feature of the metal semiconductor energy diagram at the equilibrium, as shown in **figure II.7 (d)** for the n-type semiconductor, is the appearance of a discontinuity of the allowed energy states, which results in the formation of an energy barrier at the metal/semiconductor interface, Φ_B , known as the Schottky barrier. Φ_B is the barrier against electron's flow from the metal to the n-type semiconductor and plays a similar role as Φ_i with the important difference that while Φ_i can be modified by the application of an external voltage bias, Φ_B is unaffected by the voltage bias. Φ_B is called the Schottky barrier height (SBH) and can be related to the metal workfunction and to the semiconductor electron affinity, as shown in **figure II.7(d)** [92], [93]:

$$\Phi_B = \Phi_M - \chi = \Phi_i + (E_c - E_f) \quad (\text{II.12})$$

The Schottky photodiodes are operated under a reverse bias condition. Thus, a very small current flows in the external circuit under dark condition. When the device is exposed to illumination, excess electron-hole pairs are generated due to photoelectric effect in the device. These photo-generated excess electrons and holes are drifted in the opposite directions by the high electric field in the depletion region of the Schottky junction resulted due to the applied reverse bias voltage. The extraction of photogenerated electrons and

holes results in a significant current in the circuit proportional to the intensity of the incident illumination [94].

In general, the Schottky junction photodiodes are faster and more sensitive to incident photons than the photoconductor type photodetectors. However, the selection of both the metals and photoactive materials plays crucial roles in determining the performance of the Schottky photodetectors[94]

CHAPTER III:
Study of IZTO/ β -Ga₂O₃
Photodetector based on
Schottky Barrier Diode by
Silvaco-Atlas

III.1.Introduction :

Modelling and simulation play a key role in the optimization and development of new semiconductor devices[95]. The physical process simulation means the use of mathematical description, or model, of a real system in the form of a computer program. This model is composed of equations that duplicate the functional relationships within the real system[96], it is preferable to have exact solutions for each system in order to achieve the highest level of accuracy[95]. It is a tool that enables to analyse, predict, interpret and understand the physical phenomena governing the transport in devices (such as photodetectors) from a set of parameters and initial conditions and allows us to achieve results not achievable by other means. In addition, the study of the real behaviour of photodetector requires a detailed description of the device to simulate and materials used in its realization. The selection of the type of material and its composition as well as its electrical and physical properties are very important and directly effect on his performance[96].

For over three decades, Silvaco-Atlas has helped engineers and researchers around the world. Silvaco solutions span from atoms to systems: starting with simulation of material behavior impacting semiconductor devices, to design and analysis of devices. It is a powerful devices design simulator that provides better physics insight with realistic parameters observations, including electrical, optical and thermal properties. It is a physically based two and three-dimensional device simulator and provides insight into the internal physical mechanisms associated with device operation[5]. Physically-based simulation has become very important because of it quicker and cheaper than performing experiments, as it also provides information that is difficult or impossible to measure them empirically[97].

The objective of this chapter is to describe the simulation software Silvaco-Atlas and its implementation in the framework for Investigation of the electrical characteristics and the

photo- parameters of the solar blind photodetector based on β -Ga₂O₃ that has schottky junction structure.

III.2. Silvaco-Atlas:

Silvaco-Atlas is a physically-based device simulator. Physically-based device simulators predict the electrical characteristics that are associated with specified physical structures and bias conditions. This is achieved by approximating the operation of a device onto a two or three-dimensional grid, consisting of a number of grid points called nodes. By applying a set of differential equations, derived from Maxwell’s laws, to this grid, we can simulate the transport of carriers through a structure[97].

Silvaco Atlas contains a large number of useful modules among the most used as interactive tools DeckBuild and Tonyplot, process simulator Athena, device simulator Atlas, structure and mesh editor DevEdit as presented in **Figure III.1**[5].

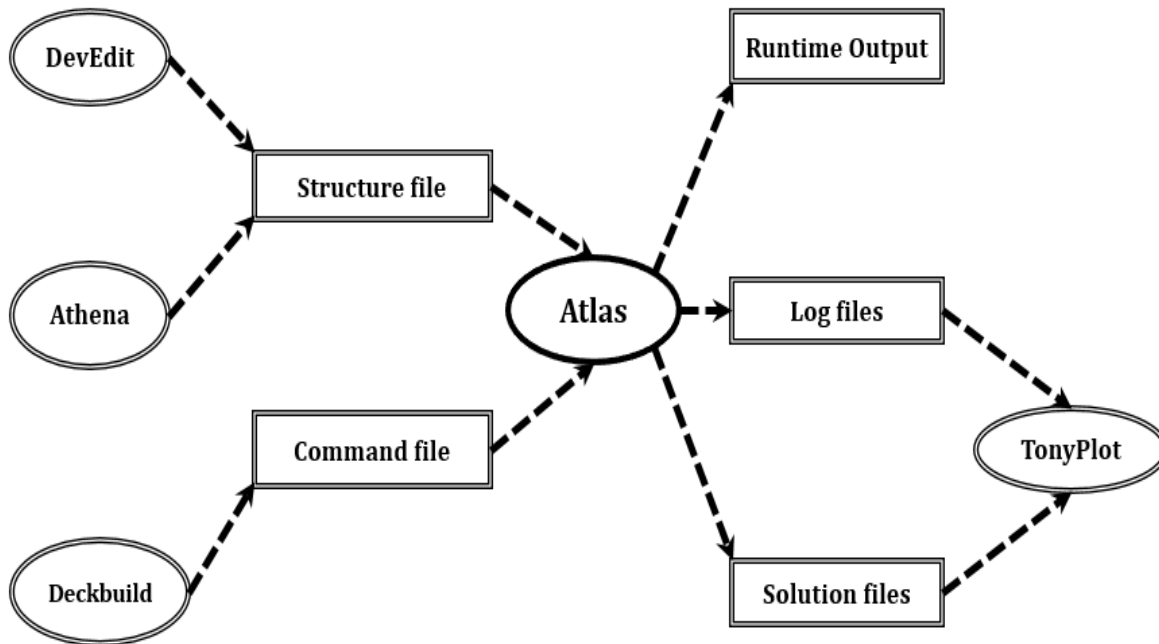


Figure III.1: Simulation flow diagram of Silvaco-Atlas

✓ **Deckbuild:** is an interactive, graphic runtime environment for developing process and device simulation input decks. It is the main window of Silvaco where all simulators can be controlled[5].

✓ **Atlas:** is a physically based device simulator module, which predicts the electrical characteristics that are associated with specified physical structures and bias conditions. This is achieved by approximating the operation of a device onto a grid (discretizing). The transport of carriers through this device can be simulated by applying a set of differential equations, derived from Maxwell's laws in this grid. This means that Atlas provides a platform to analyse AC, DC and time domain responses for all semiconductor based technologies in two and three dimensions. Atlas is also used for device generation[5].

✓ **TonyPlot:** is a graphical post-processing tool for use with all Silvaco simulators and is an integral part of the Interactive tools. TonyPlot can operate stand-alone or along with other interactive tools, such as Deckbuild. It provides scientific visualization capabilities including xy plots with linear and logarithmic axes, polar plots, surface and contour plots[5].

III.2.1.A brief of how a structure is built and simulated:

The first line to be read by the program when running Atlas using DeckBuild is the **GO ATLAS** command. After that, the structure of the statement should be followed in the sequence depicted in **figure III.2** if the order is not respected, an error message appears and the program does not execute correctly. An Atlas statement is comprised of a keyword and a set of parameters, which are not case sensitive, in the following format[96]:

<STATEMENT> <PARAMETER>=<VALUE>

Group	Statements
1. Structure Specification	Mesh Region Electrode Doping
2. Material Models Specification	Material Models Contact Interface
3. Numerical Method Selection	Method
4. Solution Specification	Log Solve Load Save
5. Results Analysis	Extract TonyPlot

Figure III.2: Command group and statements layout for a Silvaco Atlas file[5].

III.2.1.1.Mesh:

The grid consists of horizontal and vertical lines with a user-defined distance between them. It bounds the physical area of the device by creating a number of triangles in which the simulation will take place[96]. The intersections of lines are called nodes, while the spaces between them called elements[5].

we can construct a device design with 2D or 3D and can be comprised of many different sections[96]. Accurate simulation requires a smooth mesh that can resolve all significant requirements of the solution. Numerical efficiency requires a mesh that minimizes the total number of grid points thus a fast simulation. Another condition must be taken in consideration is the maximum number of nodes supported by the software; in Silvaco-Atlas, a two-dimensional simulations may support up to 100,000 nodes. Three-dimensional

simulations may support up to 20,000,000 nodes and 40,000,000 elements, with no more than 100,000 nodes in a single plane and a maximum of 2,000 planes in the z direction[5].

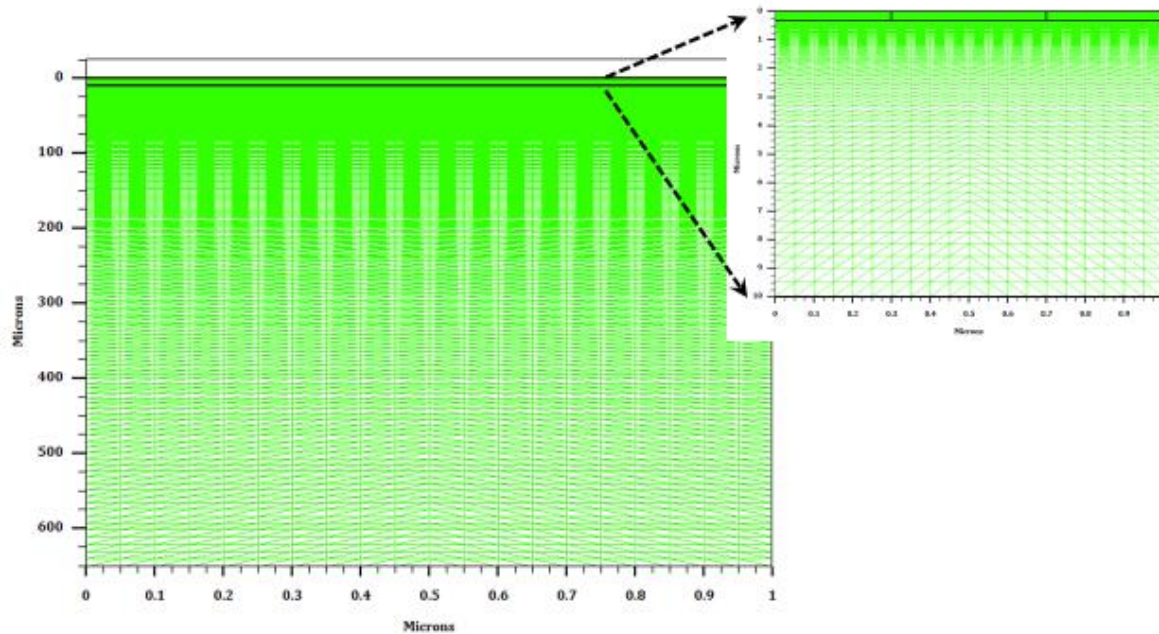


Figure III.3 :Example of a mesh Profile in a simulated device[5].

Figure III.3 shows the device's mesh of the considered example, which can be generated using the following code:

```
# X mesh

x.mesh location=0          spacing=0.5

x.mesh location=20        spacing=0.5

# Y mesh
```

```
y.mesh location=0      spacing=0.01
y.mesh location=0.3    spacing=0.001
y.mesh location=0.31   spacing=0.005
y.mesh location=10     spacing=0.5
y.mesh location=660    spacing=10
```

Where “spacing” specifies the mesh spacing at the mesh locations specified by “location” parameter[5].

III.2.1.2.Region:

The next step in creating a semiconductor device is to separate the created mesh into regions[96]. which can be realised by using the following code:

```
region number=1 user.material=air x.min=0 x.max=1 y.min=0\
y.max=0.3
```

```
region number=2 user.material=SurfaceGa2O3 x.min=0 x.max=1\
y.min=0.3 y.max=0.31
```

```
region number=3 user.material=Ga2O3 x.min=0 x.max=1 y.min=0.31\
y.max=10.3
```

```
region number=4 user.material=SnGa2O3 x.min=0 x.max=1 \ y.min=10.3
y.max=660.3
```

```
region number=5 user.material=IZTO x.min=0.2 x.max=0.8 y.min=0\
y.max=0.3
```

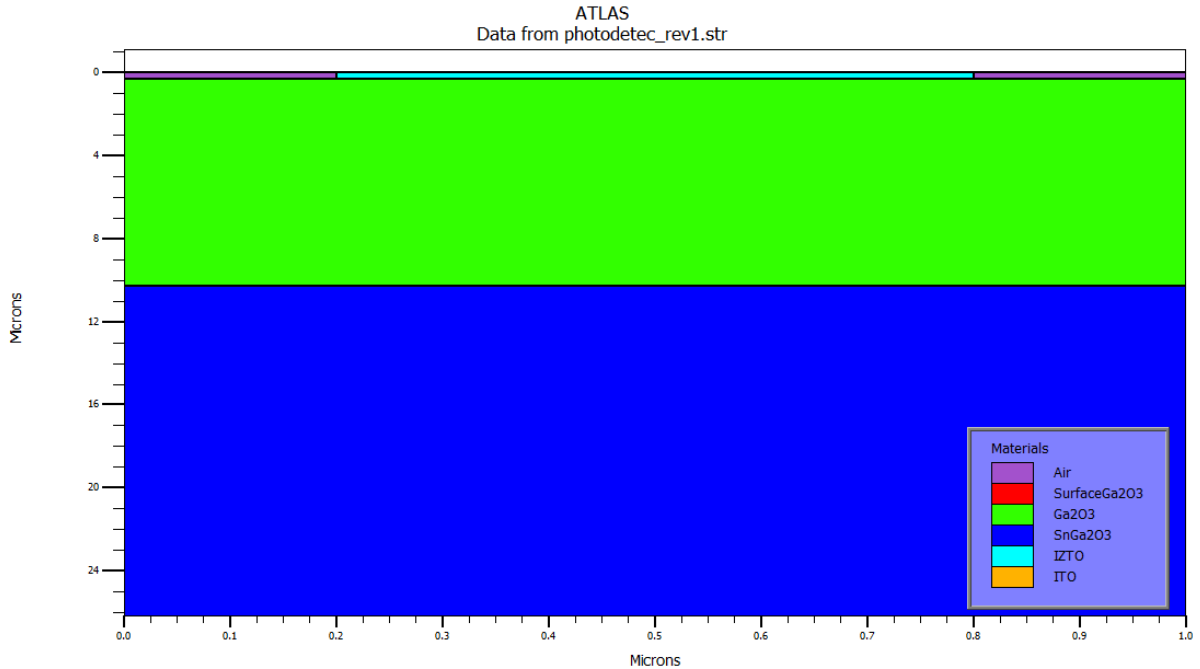


Figure III 4 : Device region specification.

III.2.1.3. Contacts :

After defining the regions and materials, the next step is to create contacts on the device. To define the electrodes of the device, their position and size need to be entered. Additional information about their materials and work functions can be supplied if needed[96]. An example format to define the electrodes is:[2]

```
Electrode name=anode material=IZTO x.min=0.2 x.max=0.8\ y.min=0
y.max=0.3
```



```
electrode name=cathode material=gold bottom
```

III.2.1.4. Doping

After creating the separate regions and assigning materials to those regions, the materials themselves can be doped. The user specifies the doping using the **DOPING** statement[96]:

```
doping conc=2.80e20 n.type uniform x.min=0.2 x.max=0.8 y.min=0\  
y.max=0.3
```

```
doping conc=3e16 n.type uniform x.min=0 x.max=1 y.min=0.3\  
y.max=10.3
```

```
doping conc=1e18 n.type uniform x.min=0 x.max=1 y.min=10.3\  
y.max=660.3
```

The **DOPING** statement is broken down into three sections: First, the distribution type can be either uniform, Gaussian, or complementary error function forms, only the uniform distribution type is utilized in this work. Next, a concentration and type of doping must be specified. Finally, the region to be doped must be identified[96].

The presence of deep defects may significantly influence the electrical characteristics of the device. Two methods are used to introduce deep levels in Atlas, depending on their spatial distribution: the “trap” statement activates bulk traps at discrete energy levels within the bandgap of the semiconductor with a uniform distribution and sets their parameter values. While the “doping” statement can be used to introduce a non-uniform traps distribution[5].

Deep levels can be defined using their activation energy, emission and capture cross section for electrons and holes and their density. These are the required parameters to define traps in Atlas, in addition to their type and location[5]. The following line of code is an example of the Atlas syntax for traps definition:

```
trap acceptor x.min=0 x.max=1 y.min=0.3 y.max=0.31\ e.level=0.75
density=0.9e16 sign=5.4e-11 sigp=5.4e-13 degen=1
```

III.2.1.5. Material

The previously defined region must be associated with specific materials. Materials used throughout the simulation can be selected from a library that includes a number of common elements, compounds, and alloys. These have their most important parameters already defined. However, in photodetectors, the use of exotic materials is not unusual. For such purposes, there is the ability to fully define already existing or brand new materials, down to their smallest detail. Such properties range from the essential bandgap and mobility all the way to light absorption coefficients. Contact information and work functions can also be entered here[96].

The general MATERIAL statement is:

MATERIAL <localization> <material definition>.

when material is not defined in the materials Silvaco library[5]. The following line of code is an example of the Atlas syntax for material definition

```
material    mat=SnGa2O3    EG300=4.8    affinity=4    user.default=GaN\
USER.GROUP=SEMICONDUCTOR    MUN=172    MUP=10    nc300=3.7e18    nv300=5e18\
permittivity=12.6    VSATN=1e7    INDX.IMAG=Ga2O3_255.k\
INDX.REAL=Ga2O3_255.n    d.tunnel=1e-5    COPT=1.1e-8    AUGN=2.8e-31\
AUGP=9.9e-32
```

III.2.1.6.Models:

More than seventy models can be used to achieve a better description of a full range of phenomena. Each model can be accompanied by a full set of its parameters when these differ from the default. we can be described a new model using the C interpreter capability[2]. The general MODELS statement is:

MODELS <model name>.

III.2.1.7.Numerical method selection:

The device electrical properties are modelled using numerical solutions of fundamental partial differential equations that link the electrostatic potential with the carrier densities. For each mesh point of a given device, Atlas solves a system of three partial differential equations, which are the Poisson's equation and the holes and electrons equations of continuity. Atlas produces numerical solutions by calculating the values of the unknowns at each grid point of the device. Atlas provides several numerical methods to calculate the solutions of semiconductor device problems[5]. There are three main types of numerical methods. The first method is the **GUMMEL** type, which is useful where the system of equations is weakly coupled but has only linear convergence. The next method is **NEWTON**, which is useful when the system of equations is strongly coupled and has quadratic convergence. This method causes Atlas to spend extra time solving for quantities, which are essentially constant or weakly coupled and requires a more accurate initial guess to the problem to obtain convergence. The final method is the **BLOCK** method, which can provide faster simulation times in situations where the NEWTON method struggles. Numerical methods are given in the **METHOD** statements of the input file. An example of an efficient METHOD statement is:

METHOD GUMMEL BLOCK NEWTON[96]

III.2.1.8.Solution specification:

This section of the input deck to Atlas is where the simulation does its calculations to solve for the device specified. It is divided up into four parts: **LOG**, **SOLVE**, **OUTPUT** and **SAVE** [96],[5]:

✓ **The LOG:**

The statement creates a save file where all results of a run will be saved; Any DC, transient or AC data generated by **SOLVE** statements after the **LOG** statement will be saved. An example **LOG** statement in which data is saved into example.log is[96]:

LOG OUTFILE = example.log

✓ **The SOLVE:**

SOLVE statement follow the **LOG** statement and instructs Atlas to perform a solution for one or more specified bias points after getting an initial guess by solving the only Poisson equation, which means a simplified initial solution. An example **SOLVE** statement that ramps the anode voltage from 0.0 V to 3.0 V with 0.01 V steps w is[96],[5]:

```
solve init
solve vanode=0 vstep=0.01 vfinal=3 name=anode
```

✓ **OUTPUT and SAVE:**

Some of the obtained results have different values along the structure (distribution) such as electron and hole densities, potential ...etc. this requires a structural presentation. For that purpose, Atlas provides the possibility of saving these data into a structure file (**.str**) using the **SAVE** statement. An example of the **SAVE** statement which stores the data into a file named (Schottky.str) is:

save outf= Schottky.str

III.2.1.9.Data Extraction and Plotting:

After saving the results and the structure, the next step is the Data Extraction and Plotting through the extraction of the saved files. The extraction is based on two methods, the first is the extraction as data and the other type is through figures. The two statements associated with this section are **EXTRACT** and **TONYPLOT**[96],[5].

✓ Extract:

For data extraction, **EXTRACT** command is provided within the DeckBuild environment. It allows to extract device parameters. The command has a flexible syntax that allows to construct specific extract routines. **EXTRACT** operates on the previous solved curve or structure file. By default, **EXTRACT** uses the currently open log file. To override this default, the name of a file to be used by **EXTRACT** is specified before the extraction routine. The **EXTRACT** statement is:

EXTRACT INIT INF="<filename>".

For example, the following command is used for current versus voltage extraction:

```
extract name="IV" curve(v."anode",i."cathode") outfile="IV.dat"
```

✓ **TonyPlot:**

For plotting the results, **TonyPlot** graphical post processing tool is used. The command **TonyPlot** is used in Deckbuild after saving data and structure. Then the name of the file is specified as presented in the following example[5]:

```
tonyplot Schottky.str
```

```
tonyplot IV.dat
```

The first command is used for the structure plot and the second for current versus voltage data plot[5].

III.3.Device structure and physical models:

III.3.1.Device structure :

The Schottky barrier ultraviolet photodetector (SD-UV PhD) based on β -Ga₂O₃ studied is shown in **figure III.5**. It consisted of the Schottky barrier diode structure which consists of a 300 nm InZnSnO (IZTO), was deposited on the top of Si-doped β -Ga₂O₃ which is used due to its high purity and provides a low resistance, a low on-resistance and a high breakdown voltage[5]. It deposited on a Sn-doped β -Ga₂O₃ substrate which is used as a drift layer with InSnO (ITO) as an ohmic contact[5]. The thicknesses of Si-doped β -Ga₂O₃ and Sn-doped β -Ga₂O₃ are 10 and 650 μ m while their doping are $3 \times 10^{16} \text{cm}^{-3}$ and $1 \times 10^{18} \text{cm}^{-3}$, respectively.

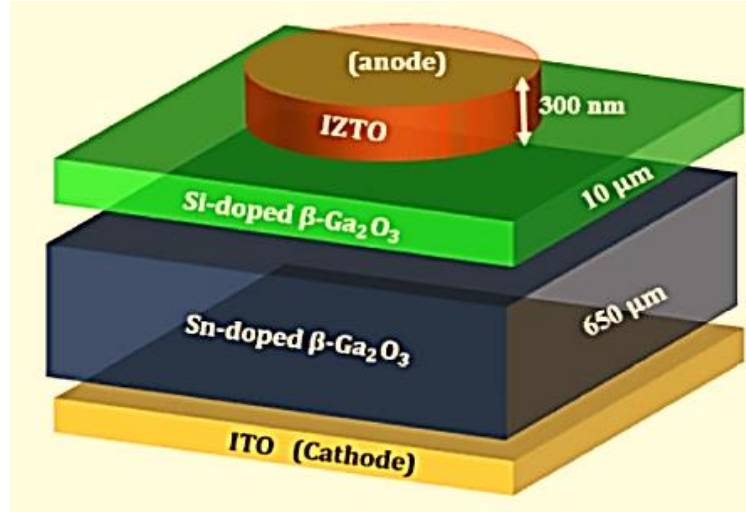


Figure III.5 : A schematic representation of the β -Ga₂O₃ Schottky barrier diode (SBD) structure[98].

Table III.1 : Physical input material parameters in the simulation process.

Parameters	Sn: β -Ga ₂ O ₃	Si: β -Ga ₂ O ₃
Band gap(eV)	4.8	4.8
Affinity(eV)	4	4
Hole mobility(cm ² /V s)	10	10
Electron mobility(cm ² /V s)	172	300
Relative permittivity	12.6	11
N _c (cm ⁻³)	3.7×10^{18}	3.7×10^{18}
N _v (cm ⁻³)	5×10^{18}	5×10^{18}
N _d (cm ⁻³)	1×10^{18}	3×10^{16}
Saturation velocity (cm/s)	10^7	10^7

Table III.2 : Input trap parameters in the simulation process.

Traps	Traps level ($E_c - E$)(eV)	Concentration (cm ⁻³)	Capture cross section σ_n (cm ²)	σ_n/σ_p
Sn-doped β- Ga₂O₃ bulk layer	0.55	4.9×10^{16}	5.4×10^{-11}	100
	0.74	4.5×10^{17}	0.5×10^{-11}	100
	1.04	5×10^{17}	2×10^{-11}	100
Si-doped β- Ga₂O₃ thin layer	0.75	1.3×10^{16}	5.4×10^{-11}	100
	1.05	1×10^{16}	2×10^{-11}	100

III.3.2. Optical and Electrical Properties of IZTO Thin Film:

Transparent conducting oxide (TCO) films have been widely used as transparent electrodes of various optoelectronic devices . multicomponent TCO materials have been reported as anode materials. Among the various materials, IZTO films have gained much attention as anode materials due to their high work function, good conductivity, high transparency, and low deposition temperature[99].

The obtained resistivity, carrier concentration, workfunction, and mobility of IZTO were $4.86 \times 10^{-4} \Omega \cdot \text{cm}$, $2.80 \times 10^{20} \text{ cm}^{-3}$, 4.79 eV, and $10.83 \text{ cm}^2/\text{V}\cdot\text{s}$, respectively. Figure 2a shows the main optical properties of IZTO thin film:

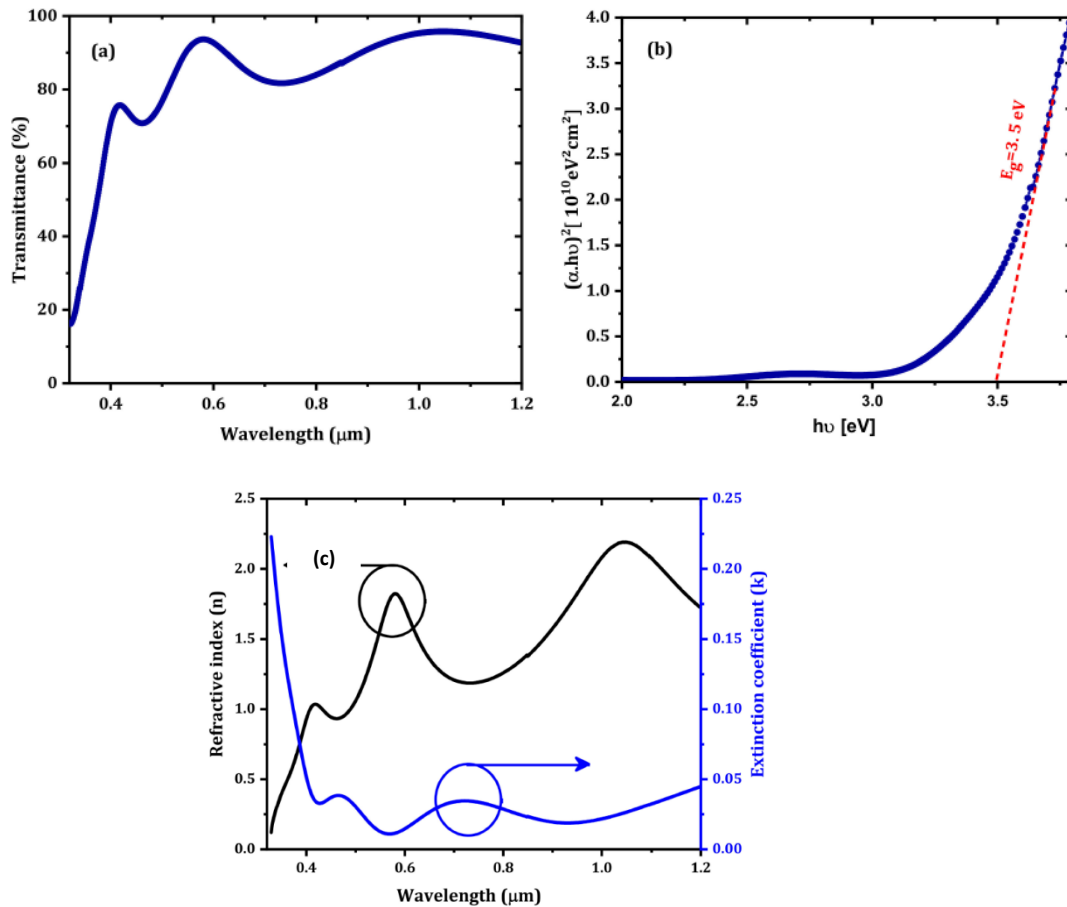


Figure III.6 : Main optical properties of IZTO thin film[98]

Therefore, the IZTO properties are making this material suitable as a metal (anode) in Schottky contact with β -Ga₂O₃. In particular its transmittance as we show in the figure III.6(a) it has a good transmittance from UV to visible wavelengths (the visible wavelength range was over 87%[98]).

As we know the IZTO is hard to deposit on β -Ga₂O₃ because of mismatch between them. So as a solution, we can Dope the surface of β -Ga₂O₃ with silicon carbide (SiC) can potentially aid in the deposition of IZTO by improving the compatibility between the two materials. This help to reduce lattice mismatch and enhance the adhesion of IZTO during the deposition process.

Table III.3 : Main IZTO properties for simulation :

Parameters	IZTO
Electron mobility(cm ² /V s)	10.83
Eg(eV)	3.6
Work function (eV)	4.79

III.3.3.The used physical models:

The simulation is carried out using Silvaco-Atlas software. Basically, Poisson's carrier continuity and drift-diffusion equations are solved in the steady state to calculate the J-V characteristics, the responsivity, and the current versus light power, while the time response is calculated in transient state with a brief light intensity. The used light source is an LED with a given wavelength (255 nm, 385 nm and 500 nm) and a power density of 1 mW/cm². In this simulation, the used physical models are: standard concentration dependent mobility, parallel field mobility, Shockley-Read-Hall (SRH), Auger and radiative recombination, Fermi-Dirac statistics and Selberherr impact ionization models[100].

First, the basic drift-diffusion semiconductor equations (Poisson equation and continuity equations for electrons and holes) are as follows[100]:

$$\text{div}(\epsilon \nabla \psi) = -q(p - n + N_d \pm N_t^\pm) \quad (\text{III.1})$$

$$0 = \frac{1}{q} \text{div} \vec{J}_n + G_n - R_n \quad (\text{III.2})$$

$$0 = -\frac{1}{q} \text{div} \vec{J}_p + G_p - R_p \quad (\text{III.3})$$

Where ψ is the electrostatic potential, ϵ is the permittivity, p and n are free holes and electron concentrations, respectively, and N_t^\pm is the ionized trap density (cm^{-3}). G_n and G_p are the generation rates for electrons and holes, R_n and R_p are the recombination rate for electrons and holes \vec{J}_n and \vec{J}_p are the electron and hole current density which given[98]:

$$\vec{J}_n = q\mu_n n \mathbf{E} + \mu_n K T \nabla n \quad (\text{III. 4})$$

$$\vec{J}_p = q\mu_p p \mathbf{E} - \mu_p K T \nabla p \quad (\text{III. 5})$$

For modelling this structure, different physical models were used:

III.3.3.1. standard concentration dependent mobility model:

The standard concentration dependent mobility model is a commonly used model in semiconductor device simulation. This model express the effect of scattng mechanisms including lattice vibrations (phonons), impurity ions, other carriers, surfaces, and other material imperfections on carrier mobility.

Since the effects of all of these microscopic phenomena are lumped into the macroscopic mobilities introduced by the transport equations, these mobilities are therefore functions of the local electric field, lattice temperature, doping concentration, and so on. The concentration dependent mobility parameter is the model that links the mobility to the concentration of dopants. This model includes the effects of lattice scattering, impurity scattering (with screening from charged carriers), carrier-carrier scattering, and impurity clustering effects at high concentration as follow[5]:

$$\frac{1}{\mu_{n,p}} = \frac{1}{\mu_{n,pL}} + \frac{1}{\mu_{n,p \text{ DAP}}} \quad (\text{III.6})$$

$\mu_{n,p}$ are the total electron and hole mobilities, $\mu_{n,pL}$ are the electron and hole mobilities due to lattice scattering, $\mu_{n,p \text{ DAP}}$ are the electron and hole mobilities due to donor (D), acceptor (A), screening (P) and carrier-carrier scattering.

III.3.3.2.Parallel field mobility model:

As carriers are accelerated in an electric field, their velocity will begin to saturate when the electric field magnitude becomes significant. This effect has to be accounted for by a reduction of the effective mobility since the magnitude of the drift velocity is the product of the mobility and the electric field component in the direction of the current flow. This model expresses the parallel electric field mobility dependence as[5]:

$$\mu_n(\mathbf{E}) = \mu_{n0} \left[\frac{1}{1 + \left(\frac{\mu_{n0} E}{v_{\text{satn}}} \right)^{\gamma_n}} \right]^{\frac{1}{\gamma_n}} \quad (\text{III.7})$$

Where v_{satn} is the electron saturation velocities, γ_n is a user-definable parameter in this model ($\gamma_n = 2^{30}$), μ_{n0} is low-field electron and mobilities, E is the parallel electric field [100].

III.3.3.3.Shockley-Read-Hall (SRH) model:

To take account of recombination effects, we recommend the use of the Shockley-Read-Hall (SRH) model. This simulates the leakage currents that exist due to thermal generation[101].

Traps are represented by their ionized density N_t^\pm . The sign \pm depends on whether the trap is an acceptor or a donor, so that $N_t^+ = f \cdot N_t$ and $N_t^- = (1 - f)N_t$. f is the occupancy function given by $f = \frac{\sigma_n n + \sigma_p p}{\sigma_n(n+n_t) + \sigma_p(p+p_t)}$. $\sigma_{n(p)}$ is the trap capture cross-section for electrons (holes).

$R_{SRH} = R_{n,p} = \frac{pn - n_i^2}{\tau_{0n}(p+p_t) + \tau_{0p}(n+n_t)}$ where $n_t = n_i \exp(-(E_i - E_t)/KT)$ and $p_t = n_i \exp(-(E_t - E_i)/KT)$ and τ_{0n} and τ_{0p} are the minority carrier lifetimes which are also related to the traps through $\tau_{0n(p)} = \frac{1}{v_{thn(p)} \sigma_{n(p)} N_t}$ where $v_{thn(p)}$ is the thermal velocity of electrons (holes)[98].

III.3.3.4. Auger recombination

The Auger recombination is a bimolecular recombination where, the released energy during the recombination of an electron and a hole is not an emission of a photon but, instead, it is transferred to a third particle (electron or a hole). The energy is eventually transferred non-radiatively from the hot third carrier via phonon emission to the lattice. Auger Recombination is commonly modelled using the expression[5]:

$$\mathbf{R}_{Auger} = \gamma_n (\mathbf{p} \cdot \mathbf{n}^2 - \mathbf{n} \cdot \mathbf{n}_i^2) + \gamma_p (\mathbf{n} \cdot \mathbf{p} - \mathbf{p} \cdot \mathbf{n}_i^2) \quad (\text{III. 8})$$

Where γ_n and γ_p are the Auger coefficients (cm⁶/s).

However, the radiative direct recombination is usually given by the expression[100]:

$$\mathbf{R}_{np} = \mathbf{C}_{np} (\mathbf{pn} - \mathbf{n}_i^2) \quad (\text{III. 9})$$

Where \mathbf{C}_{np} is a model parameter characteristic of β -Ga₂O₃.

The total recombination is the sum of individual recombination, that is[100]:

$$\mathbf{R} = \mathbf{R}_{Auger} + \mathbf{R}_{SRH} + \mathbf{R}_{np} \quad (\text{III.10})$$

III.3.3.5.Selberherr's impact ionization

The Selberherr's impact ionization model is used to describe the avalanche breakdown effect. The avalanche breakdown process occurs when electrons and/or holes, moving across the space charge region, acquire sufficient energy from the electric field to create electron-hole pairs by colliding with atomic electrons within the depletion region. The avalanche process is schematically shown in **figure III.7**. The newly created electrons and holes move in opposite directions due to the electric field and thereby create a reverse-biased current. In addition, the newly generated electrons and/or holes may acquire sufficient energy to ionize other atoms, leading to the avalanche process. For most PN junctions, the predominant breakdown mechanism is the avalanche effect[5].

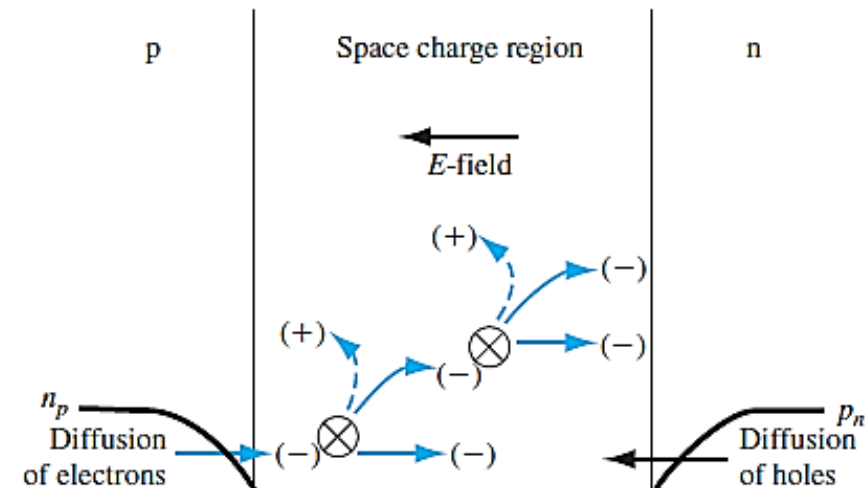


Figure III.7 :Avalanche breakdown process in a reverse-biased PN junction.

Selberherr's Impact ionization (SELB) model used for avalanche breakdown is defined through the following coefficients for electrons and holes[5]:

$$\alpha_n = A_n \exp\left(-\left(\frac{B_n}{E}\right)^{\beta_n}\right) \quad (\text{III.11})$$

$$\alpha_p = A_p \exp\left(-\left(\frac{B_p}{E}\right)^{\beta_p}\right) \quad (\text{III. 12})$$

Where E is the electric field in the current direction and A_n , A_p , B_n , B_p , β_n and β_p are fitting parameters.

III.3.3.6. Universal Schottky Tunneling (UST) model:

The tunnelling model was considered using Universal Schottky Tunneling (UST) model and the tunneling current is given by[5]:

$$J_T = \frac{A^* T_L}{K_B} \int_{\epsilon}^{\infty} \Gamma(E') \ln\left(\frac{1+F_s(E')}{1+F_m(E')}\right) dE' \quad (\text{III. 13})$$

Where A^* , T_L , K_B , ϵ , $F_s(E')$ and $F_m(E')$ are effective Richardson's coefficient, lattice temperature, Boltzmann constant, electrons energy, and the Maxwell-Boltzmann distribution in β -Ga₂O₃ and Ni, respectively. and $\Gamma(E')$ is the tunnelling probability, which is given by [102]:

$$\Gamma(\epsilon) = \exp\left[-2 \frac{\sqrt{2m^*}}{\hbar} \int_{x_1}^{x_2} \sqrt{E_c(x) - \epsilon} dx\right] \quad (\text{III.14})$$

Here, $E_c(x)$ and (x_1, x_2) are the potential energy distribution of Schottky barrier diode and classical turning points, respectively[5].

III.3.3.7. Thermionic emission model :

In Schottky barriers, the thermionic emission is also considered, and this current density is given by [5]:

$$J_{Th} = J_s \left(\exp\left(\frac{q(V-R_s I)}{\eta K_B T}\right) - 1 \right) \quad (\text{III.15})$$

Where J_s is the saturation current density, q is the elementary charge, R_s is the series resistance and η is the ideality factor. K_B and T are Boltzman constant and the absolute temperature (K), respectively. In this conduction mechanism, J_s is given by:

$$J_s = A^* T^2 \exp\left(-\frac{q\phi_B}{K_B T}\right) \quad (\text{III.16})$$

Where A^* is the Richardson constant ($41.11 \text{ A.cm}^{-2}\text{K}^{-2}$ for β -Ga₂O₃ and ϕ_B is the Schottky barrier height).

The thermionic emission model was used to analyze the current-voltage characteristics of a photodetector in the dark condition[103].

III.3.3.8.Fermi-Dirac statistics:

Electrons in thermal equilibrium at temperature T with a semiconductor lattice obey Fermi-Dirac statistics. That is, the probability $f(E)$ that an available electron state with energy E is occupied by an electron is[100]:

$$f(E) = \frac{1}{1 + \exp\left(\frac{E - E_F}{kT}\right)} \quad (\text{III.17})$$

Where E_F is the Fermi level.

III.4. Results and discussion :

The simulation is carried out using Silvaco-Atlas software. Basically, Poisson's carrier continuity and drift-diffusion equations are solved in the steady state to calculate the following characteristics:

III.4.1. Current density-Voltage (J-V) characteristic:

The J-V characteristic of a photodetector represents the relationship between the current density (J) and the voltage (V) that applied across the device (in our case reverse bias) under illumination conditions (in our case we used a light source is an LED with a given wavelength (255 nm, 385 nm and 500 nm) with a power density of 1 mW/cm²).

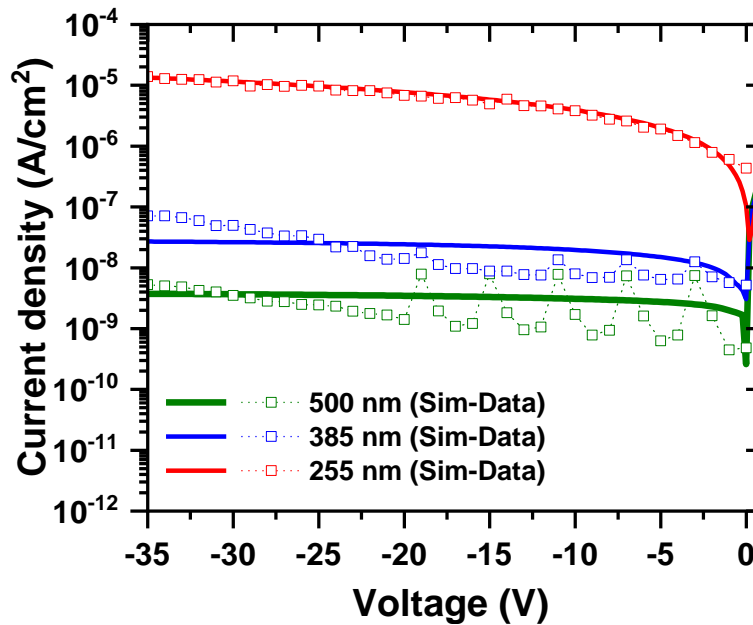


Figure III.8 : The J-V characteristic at reverse bias simulated at different wavelengths (solid lines) of the fully transparent β -Ga₂O₃ SD UVPhD compared to measurements (symbols). Each wavelength corresponds to an LED light source of 1 mW/cm²

Figure III.8 shows the simulated reverse J-V characteristic compared to measurements. This characterisation exhibits certain parameters which provide important information about the performance of this device.

The photocurrent refers to the electric current generated by the photodetector; when a photon with sufficient energy strikes the photodetector which defined as:

$$I_{ph} = I_{light} - I_{dark} \quad (III. 18)$$

It represented as the current under illumination at different applied voltages.

It is noticed that the photocurrent is crucially limited by both photogeneration and recombination process. For recombination, it seems that densities of defects that gave the best fitting with experimental curves for all wavelengths (255 nm, 385 nm and 500 nm) are quite high. However, this can be justified regarding the high doping of the bulk region (10^{18}cm^{-3}). Consequently, it was necessary to ensure a careful input of the optical indexes n and k to extract the exact absorption[100].

For better performance of photodetectors, a high photo to dark current ratio (PDCR) value is desired. It is defined by the following relationship[103]:

$$\text{PDCR} = \frac{I_{\text{ph}} - I_{\text{dark}}}{I_{\text{dark}}} \quad (\text{III.19})$$

A good light-to-dark ratio is obtained that exceeds 10^3 which is comparable to other reported β -Ga₂O₃ UV-PDs. The good light-to-dark ratio can be related to the full transparency and the thick-bulk device which significantly reduces any optical losses by reflection or transmission[100].

III.4.2.Responsivity:

Figure III.9 shows the responsivity of the β -Ga₂O₃ SD UV-PhD at different reverse bias voltages, extracted from the J-V characteristics. It depends on wavelength, optical power and applied bias.

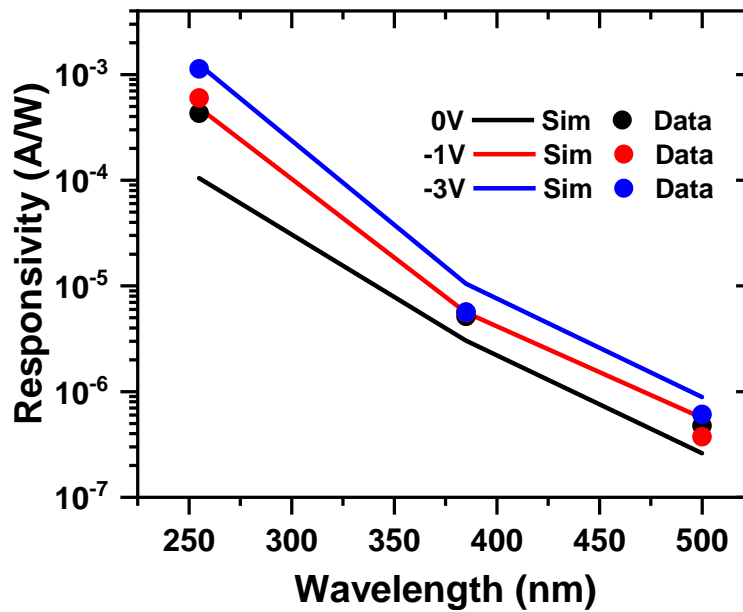


Figure III.9: Responsivity versus wavelength at different reverse voltage (simulation—solid lines) (measurements—symbols).

An acceptable fitting with measurements was achieved mainly for 255 nm which is the most important wavelength (included in the solar-blind region). At 255 nm, the device exhibited a good responsivity in the range (10^{-4} - 10^{-3} A/W). The responsivity decreases when the wavelength increase [100].

The dependence of the photocurrent on the light power density is plotted in **figure III.10** for 255 nm and -1 V.

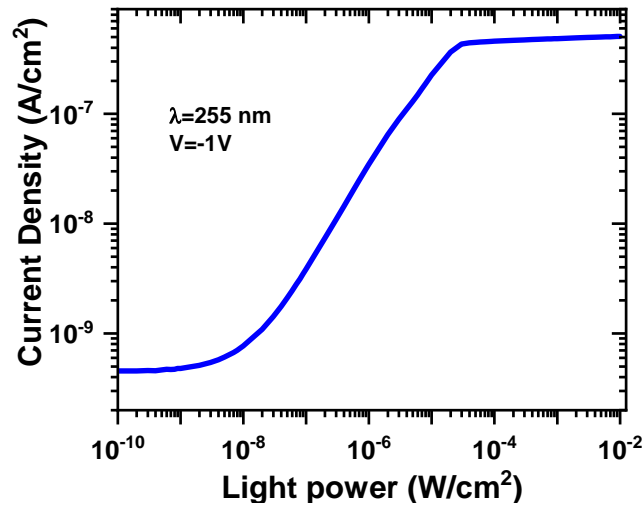


Figure III.10 : Photocurrent density versus light power density for 255 nm and at -1 V.

The I_{ph} curve gives an estimation of the device light detection ability. It is observed that the device begins to detect light with power density greater than 10^{-9} W/cm². Then, the current increases linearly on a logarithmic scale up to $\sim 5 \times 10^{-7}$ W/cm after which a saturation is established. After the termination of the light source, The persistent photoconductivity (PPC) phenomenon has often observed in heterojunction devices, and a Schottky photodiode is not an exception. This is a major issue and is generally attributed to oxygen vacancy defects resulting in shallow donor levels. Photogenerated carriers by deep UV trapped in these defect states or free holes with their low mobility form the most probable causes of the PPC phenomenon[100].

III.4.3. Response time:

Figure III.11 presents the transient response of β -Ga₂O₃ SBD UV-PhD under 255 nm

illumination (1 mW/cm^2) with a pulse width of 5 s.

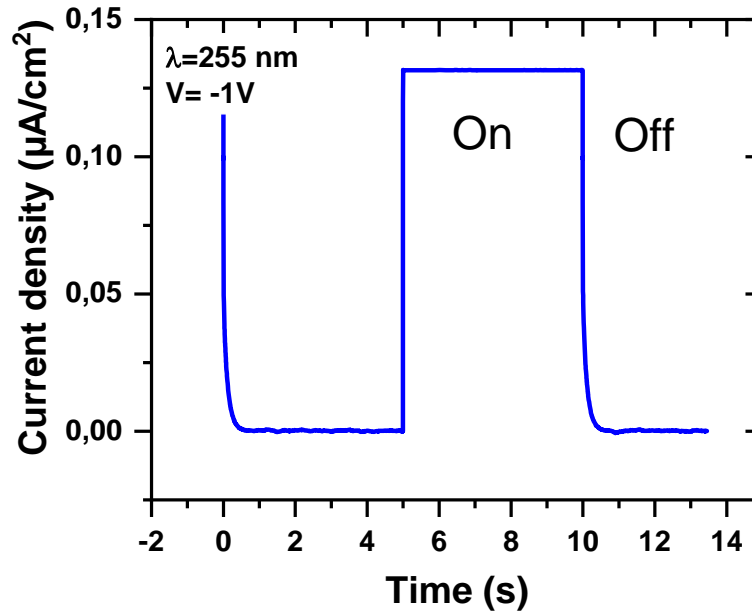


Figure III.11 : The time-dependent photoresponse under pulsed illumination of 255 nm at -1 V .

From this curve, the decay time is 0.15 s, it considered a slow decay time. There are many theories are researching the main causes that make this decay time slow including: recombination that caused by defects in the β -Ga₂O₃ (particularly the deep level defects) or the IZTO layer. Also, it is suggested that negatively charged traps near the metal-semiconductor interface can capture photogenerated holes and thus reduce the Schottky barrier height upon illumination, while the reoccupation of traps and the recovery of Schottky barrier cause the long decay time after switching off the illumination[13]. It is suggested that the reduced oxygen vacancy concentration and the increased Schottky barrier height jointly contribute to the faster response speed[13]. The device exhibits a stable off-and-on state under dark and light conditions. Furthermore, the switching

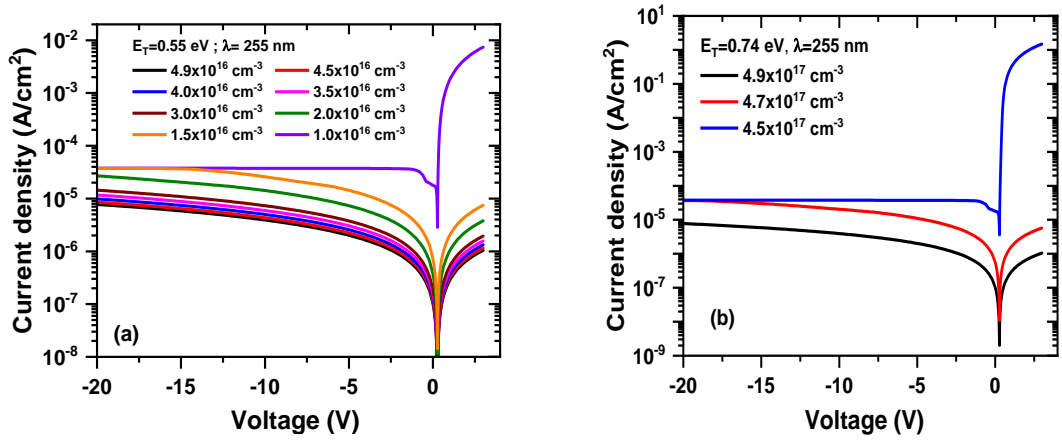
characteristics can be well maintained even at a very low working voltage (-1 V)[100].

III.4.4.Effect of bulk traps :

In this section, we will study the effect of the reduction of the bulk defects on the response performance.

III.4.4.1.The effect on J-V characteristic:

Figure III.12 (a), (b) and (c) shows the effect of $E_T = 0.55$ eV, $E_T = 0.74$ eV and $E_T = 1.04$ eV traps on generated photocurrent produced under 255 nm wavelength, respectively. These curves show the effect of the reduction of each electron trap density one by one (while keeping the two other constants at their initial high values) on the J-V characteristic.



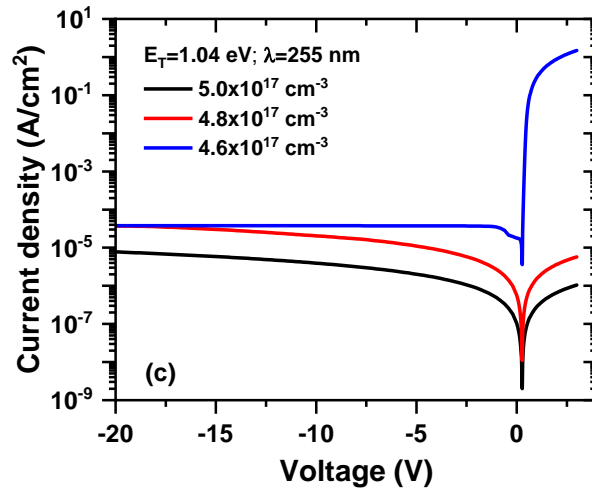


Figure III.12 : The effect of bulk trap reduction (electron traps) present in the band gap energy of β -Ga₂O₃, (a) $E_T = 0.55$ eV, (b) $E_T = 0.74$ eV and (c) $E_T = 1.04$ eV on the J-V characteristics.

According to the obtained results, the deeper position defect has the dominant influence and this is obvious since whenever the trap is deeper, the ratio of happening recombination process is high[100]. For each type of defect there is a limit density below which no further improvement occurs (10^{18}cm^{-3} for the $E_T = 0.55$ eV, $4.5 \times 10^{17} \text{cm}^{-3}$ for the $E_T = 0.74$ eV and $4.6 \times 10^{17} \text{cm}^{-3}$ for the $E_T = 1.04$ eV). In this case, the symmetric shape of the J-V characteristic is mislaid between reverse and forward bias, clearly showing the rectifying behaviour of a diode[100].

Figure III.13 represents the effect of defect density reduction on the photocurrent versus light power density. According to the obtained results, we find that as the defect density decreases, the saturation zone (controlled mainly by recombination) of the current is reduced until it disappears completely and the linear current dependency dominates the whole variation with the light power density. This means that the saturation zone is dominated by SRH recombination compared to direct and Auger recombination[100].

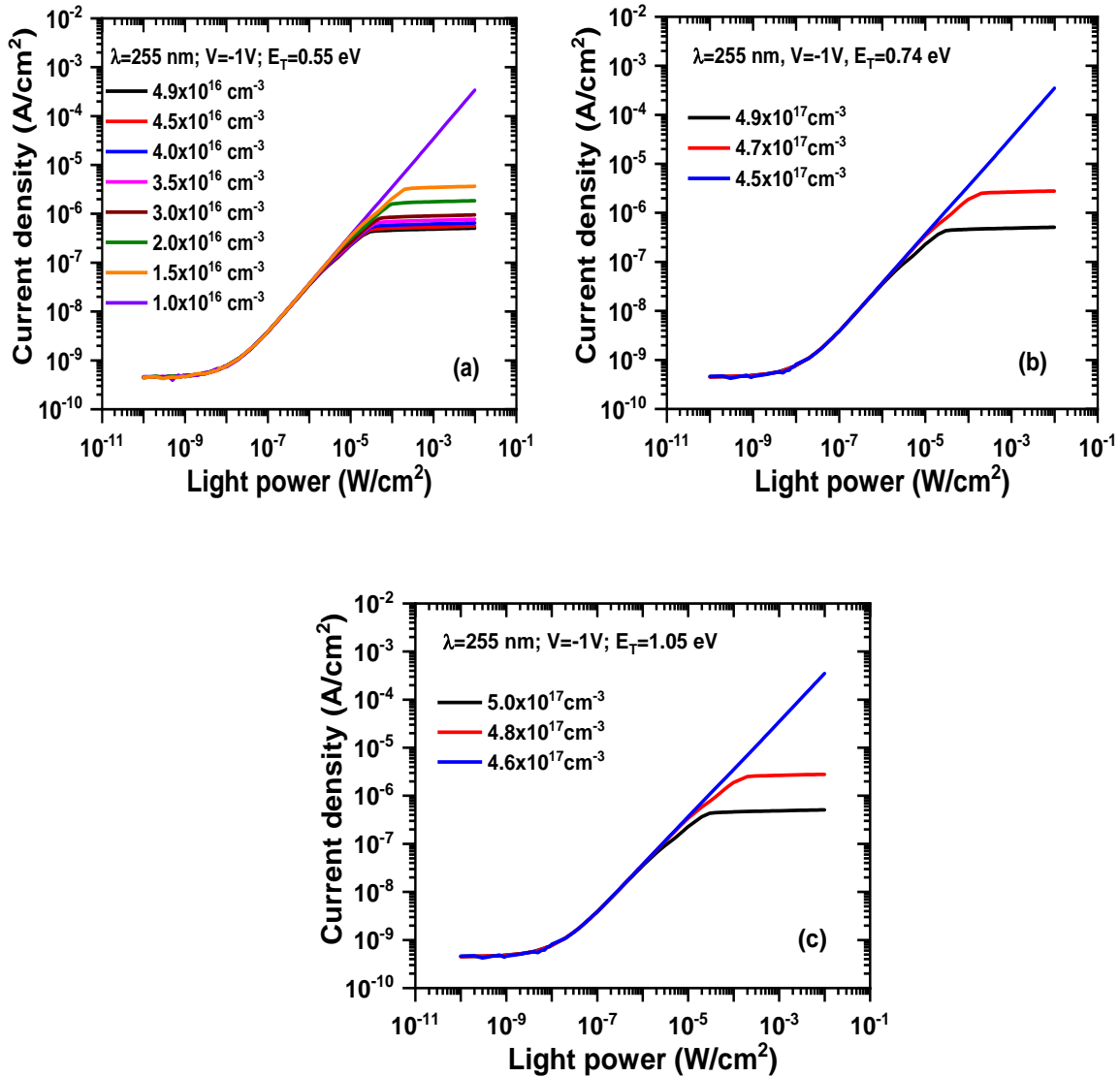


Figure III.13 : The effect of the reduction defects densities(one by one), (a) $E_T = 0.55$ eV, (b) $E_T = 0.74$ eV and (c) $E_T = 1.04$ eV on Photocurrent density versus light power density of β -Ga₂O₃ solar blind UV-PD.

III.4.4.2..The effect on Response time:

Figure III.14 represents the effect of traps reduction on the response by exposing it to a brief light pulse of 0.1 s is now examined.

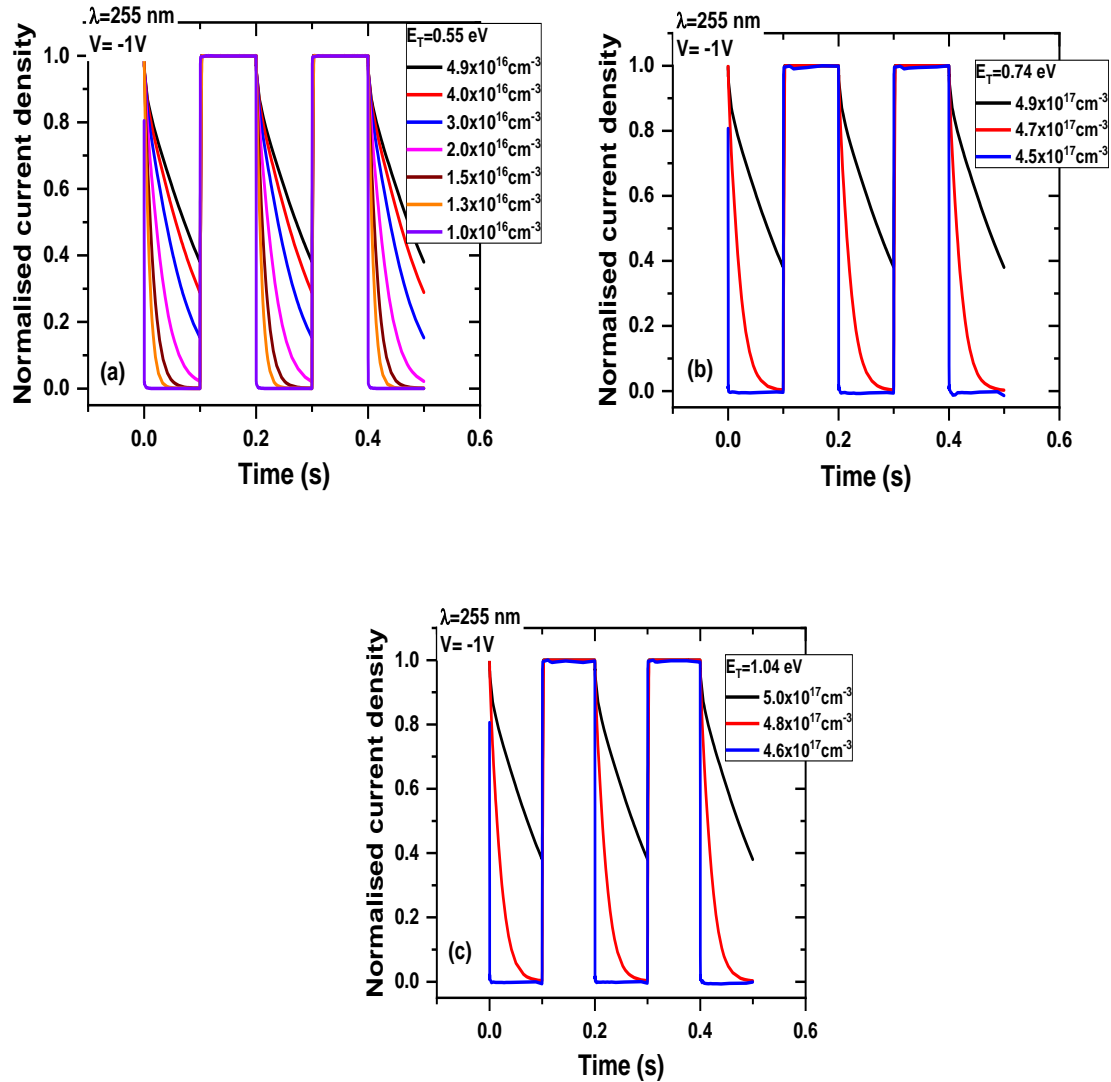


Figure III.14 : The effect of defect reduction on time-dependent photoresponse under short-pulsed illumination of 255 nm at -1 V: (a) $E_T = 0.55$ eV, (b) $E_T = 0.74$ eV and (c) $E_T = 1.04$ eV

According to the results, we find that The decay time estimated for $E_T = 0.55$ eV is ~ 0.019 s. However, for $E_T = 0.74$ eV is ~ 0.38 s and for $E_T = 1.04$ eV is ~ 0.099 s.

So, we conclude that the shallowest traps had the dominant influence ($E_T = 0.55$ eV)[100].

III.5.Conclusion:

The J-V characteristics of an IZTO/ β -Ga₂O₃ Schottky barrier diode was simulated by SILVACO-Atlas and compared with measurements. We studies also the responsivity, and the response time of this photodetector. After that we studied the effect of bulk traps on J-V characteristic and response time.

After that, we studied the effect of reducing traps densities. We observed that this helps to reduce the saturation zone current; this because of the reduce of recombination process when we reduce the deep trap densities (0.74 eV and 1.04 eV). We noticed also that this helps to solve a big problem in this device which is the slow decay time because as the defect density decreases in shallow traps(0.55eV), the recombination process will decrease in these levels .That make the decay time more faster.

Conclusion

Schottky barrier diode IZTO/ β -Ga₂O₃ photodetector has attracted great attention in UV photodetection technology, solar blind regions particularly. The study is based on numerical simulation by Silvaco-Atlas, which is a powerful software for 2D, and 3D electronic device modelling. The simulated results are also compared with available measurements.

The study included the J-V characteristic which represents the relationship between the current density (J) and the reverse bias voltage (V) under illumination conditions (a LED with a given wavelength (255 nm, 385 nm, and 500 nm) with a power density of 1 mW/cm²). We noticed that each wavelength has a photocurrent value, for 255 nm, its photocurrent has a maximum value more than the other wavelengths (385 nm and 500nm). Therefore, we can say that this photodetector is sensitive to $\lambda=255\text{nm}$ (which belongs to the solar blind region). In addition, It is noticed that the photocurrent is crucially limited by both photogeneration and recombination processes. Responsivity has been studied, we observed that the device exhibited good responsivity in the range 10^{-4} - 10^{-3} A/W. This insures the strong sensitivity to the solar blind wavelengths. Photocurrent density versus light power density curve for 255 nm and at -1 V gave us an important observation which is: at high intensity, it is expected that the incident light power and generated photocurrent do not exhibit a linear relationship, and the photodiode is saturated. This is possibly due recombination processes, thus excess photons will not be absorbed. Additionally, we studied the response time characteristic. We have concluded from its curve that the decay time is slow (0.15 s) and this is due to the recombination process in the shallow defects level.

We studied also the effect of bulk traps reduction. We conclude from the simulation that when we decrease the defect density in deep traps (0.74 eV and 1.04 eV), we notice that the saturation zone current is reduced due to decrease of the recombination process. In

addition, when we decrease the defect density in shallow traps (0.55eV), the related recombination process decreases and make the decay time faster. Furthermore, with decreasing trap densities, this PhD can be considered as a self-powered solar-blind photodiode(SBPhD).

References :

- [1] X. Chen, F. Ren, S. Gu, et J. Ye, « Review of gallium-oxide-based solar-blind ultraviolet photodetectors », *Photon. Res.*, vol. 7, n° 4, p. 381, avr. 2019, doi: 10.1364/PRJ.7.000381.
- [2] A. Rogalski, Z. Bielecki, J. Mikołajczyk, et J. Wojtas, « Ultraviolet Photodetectors: From Photocathodes to Low-Dimensional Solids », *Sensors*, vol. 23, n° 9, p. 4452, mai 2023, doi: 10.3390/s23094452.
- [3] Z. Yan *et al.*, « High sensitivity and fast response self-powered solar-blind ultraviolet photodetector with a β -Ga₂O₃/spiro-MeOTAD p-n heterojunction », *J. Mater. Chem. C*, vol. 8, n° 13, p. 4502-4509, 2020, doi: 10.1039/C9TC06767A.
- [4] Y. Wang *et al.*, « Realization of cost-effective and high-performance solar-blind ultraviolet photodetectors based on amorphous Ga₂O₃ prepared at room temperature », *Materials Today Advances*, vol. 16, p. 100324, déc. 2022, doi: 10.1016/j.mtadv.2022.100324.
- [5] M. Labeled, « Study of Schottky diodes based on ultrawide-band gap semiconductors », Mohamed Khider University, Biskra. [En ligne]. Disponible sur: <http://thesis.univ-biskra.dz/id/eprint/5865>
- [6] T. Harada et A. Tsukazaki, « Control of Schottky barrier height in metal/ β -Ga₂O₃ junctions by insertion of PdCoO₂ layers », *APL Materials*, vol. 8, n° 4, p. 041109, avr. 2020, doi: 10.1063/1.5145117.
- [7] Sundar Babu Isukapati, « Gallium Oxide Thin Films for Optoelectronic Applications », YOUNGSTOWN STATE UNIVERSITY, 2018.
- [8] H. Xue, Q. He, G. Jian, S. Long, T. Pang, et M. Liu, « An Overview of the Ultrawide Bandgap Ga₂O₃ Semiconductor-Based Schottky Barrier Diode for Power Electronics Application », *Nanoscale Res Lett*, vol. 13, n° 1, p. 290, déc. 2018, doi: 10.1186/s11671-018-2712-1.
- [9] Liheng Zhang, « BETA GALLIUM OXIDE MATERIALS PROCESSING AND DEVICE APPLICATIONS », the Faculty of the Graduate School of Cornell University, 2017.
- [10] M.-H. Lee et R. L. Peterson, « Process and characterization of ohmic contacts for beta-phase gallium oxide », *Journal of Materials Research*, vol. 36, n° 23, p. 4771-4789, déc. 2021, doi: 10.1557/s43578-021-00334-y.
- [11] J.D. Blevins, D. Thomson, K. Stevens, and G. Foundos, « Growth of Single Crystal Beta-Gallium Oxide (β -Ga₂O₃) Semiconductor Material », p. 6, mai 2017.

- [12] L. K. Ping, D. D. Berhanuddin, A. K. Mondal, P. S. Menon, et M. A. Mohamed, « Properties and perspectives of ultrawide bandgap Ga₂O₃ in optoelectronic applications », *Chinese Journal of Physics*, vol. 73, p. 195-212, oct. 2021, doi: 10.1016/j.cjph.2021.06.015.
- [13] X. Chen, F.-F. Ren, J. Ye, et S. Gu, « Gallium oxide-based solar-blind ultraviolet photodetectors », *Semicond. Sci. Technol.*, vol. 35, n° 2, p. 023001, févr. 2020, doi: 10.1088/1361-6641/ab6102.
- [14] Bayraktaroglu, Burhan Civ AFRL/Rydd, « ASSESSMENT OF GALLIUM OXIDE TECHNOLOGY », AFRL-RY-WP-TR-2017-0167, août 2017. [En ligne]. Disponible sur: <https://apps.dtic.mil/sti/citations/AD1038137>
- [15] Y. Wang, J. Su, Z. Lin, J. Zhang, J. Chang, et Y. Hao, « Recent progress on the effects of impurities and defects on the properties of Ga₂O₃ », *J. Mater. Chem. C*, vol. 10, n° 37, p. 13395-13436, 2022, doi: 10.1039/D2TC01128J.
- [16] S. J. Pearton *et al.*, « A review of Ga₂O₃ materials, processing, and devices », *Applied Physics Reviews*, vol. 5, n° 1, p. 011301, mars 2018, doi: 10.1063/1.5006941.
- [17] S.I. Stepanov, V.I. Nikolaev, V.E. Bougrov, et A.E. Romanov, « GALLIUM OXIDE: PROPERTIES AND APPLICATION », p. 24.
- [18] P. S.] *et al.*, « A Review of Ga₂O₃ Materials, Processing and Devices », p. 237.
- [19] D. Kaur et M. Kumar, « A Strategic Review on Gallium Oxide Based Deep-Ultraviolet Photodetectors: Recent Progress and Future Prospects », *Adv. Optical Mater.*, vol. 9, n° 9, p. 2002160, mai 2021, doi: 10.1002/adom.202002160.
- [20] J. Zhang, J. Shi, D.-C. Qi, L. Chen, et K. H. L. Zhang, « Recent progress on the electronic structure, defect, and doping properties of Ga₂O₃ », *APL Materials*, vol. 8, n° 2, p. 020906, févr. 2020, doi: 10.1063/1.5142999.
- [21] M. R. Lorenz, J. F. Woods, et R. J. Gambino, « Some electrical properties of the semiconductor β-Ga₂O₃ », *Journal of Physics and Chemistry of Solids*, vol. 28, n° 3, p. 403-404, mars 1967, doi: 10.1016/0022-3697(67)90305-8.
- [22] A. Kuramata, K. Koshi, S. Watanabe, Y. Yamaoka, T. Masui, et S. Yamakoshi, « High-quality β-Ga₂O₃ single crystals grown by edge-defined film-fed growth », *Jpn. J. Appl. Phys.*, vol. 55, n° 12, p. 1202A2, déc. 2016, doi: 10.7567/JJAP.55.1202A2.
- [23] « Progress in semiconductor β-Ga₂O₃ », in *Ultra-Wide Bandgap Semiconductor Materials*, Elsevier, 2019, p. 263-345. doi: 10.1016/B978-0-12-815468-7.00003-2.

- [24] M. Mohamed *et al.*, « The surface band structure of β -Ga₂O₃ », *J. Phys.: Conf. Ser.*, vol. 286, p. 012027, mars 2011, doi: 10.1088/1742-6596/286/1/012027.
- [25] F. Shi et H. Qiao, « Preparations, properties and applications of gallium oxide nanomaterials – A review », *Nano Select*, vol. 3, n° 2, p. 348-373, févr. 2022, doi: 10.1002/nano.202100149.
- [26] R. Roy, V. G. Hill, et E. F. Osborn, « Polymorphism of Ga₂O₃ and the System Ga₂O₃—H₂O », *J. Am. Chem. Soc.*, vol. 74, n° 3, p. 719-722, févr. 1952, doi: 10.1021/ja01123a039.
- [27] M. Higashiwaki et G. H. Jessen, « Guest Editorial: The dawn of gallium oxide microelectronics », *Appl. Phys. Lett.*, vol. 112, n° 6, p. 060401, févr. 2018, doi: 10.1063/1.5017845.
- [28] M. Passlack *et al.*, « Ga₂O₃ films for electronic and optoelectronic applications », *Journal of Applied Physics*, vol. 77, n° 2, p. 686-693, janv. 1995, doi: 10.1063/1.359055.
- [29] N. S. Jamwal et A. Kiani, « Gallium Oxide Nanostructures: A Review of Synthesis, Properties and Applications », *Nanomaterials*, vol. 12, n° 12, p. 2061, juin 2022, doi: 10.3390/nano12122061.
- [30] « Binary Oxides _ Van de Walle _ Computational Materials Group _ UC Santa Barbara.html ».
- [31] W. Miller, K. Böttcher, Z. Galazka, et J. Schreuer, « Numerical Modelling of the Czochralski Growth of β -Ga₂O₃ », *Crystals*, vol. 7, n° 1, p. 26, janv. 2017, doi: 10.3390/cryst7010026.
- [32] « phd2019.pdf ».
- [33] « Labeled Madani PhD thesis- Final version 09-05-2022.docx ».
- [34] Y. Wei *et al.*, « Interaction between hydrogen and gallium vacancies in β -Ga₂O₃ », *Sci Rep*, vol. 8, n° 1, p. 10142, juill. 2018, doi: 10.1038/s41598-018-28461-3.
- [35] B. Alhalaili, H. Mao, et S. Islam, « Ga₂O₃ Nanowire Synthesis and Device Applications », in *Novel Nanomaterials - Synthesis and Applications*, G. Z. Kyzas et A. C. Mitropoulos, Éd., InTech, 2018. doi: 10.5772/intechopen.72464.
- [36] J. B. Varley, A. Janotti, C. Franchini, et C. G. Van De Walle, « Role of self-trapping in luminescence and p-type conductivity of wide-band-gap oxides », *Phys. Rev. B*, vol. 85, n° 8, p. 081109, févr. 2012, doi: 10.1103/PhysRevB.85.081109.
- [37] J.-L. Chiang, B. K. Yadlapalli, M.-I. Chen, et D.-S. Wu, « A Review on Gallium Oxide Materials from Solution Processes », *Nanomaterials*, vol.

- 12, n° 20, p. 3601, oct. 2022, doi: 10.3390/nano12203601.
- [38] M. Islam, « Study of defects and doping in β -Ga₂O₃ ».
- [39] Y. Yuan *et al.*, « Toward emerging gallium oxide semiconductors: A roadmap », *Fundamental Research*, vol. 1, n° 6, p. 697-716, nov. 2021, doi: 10.1016/j.fmre.2021.11.002.
- [40] W. B. Fowler, « Point Defects », in *Encyclopedia of Condensed Matter Physics*, Elsevier, 2005, p. 318-323. doi: 10.1016/B0-12-369401-9/00412-5.
- [41] J. B. Varley, J. R. Weber, A. Janotti, et C. G. Van De Walle, « Oxygen vacancies and donor impurities in β -Ga₂O₃ », *Appl. Phys. Lett.*, vol. 97, n° 14, p. 142106, oct. 2010, doi: 10.1063/1.3499306.
- [42] T. Zacherle, P. C. Schmidt, et M. Martin, « *Ab initio* calculations on the defect structure of β -Ga₂O₃ », *Phys. Rev. B*, vol. 87, n° 23, p. 235206, juin 2013, doi: 10.1103/PhysRevB.87.235206.
- [43] Z. Galazka, « Growth of bulk β -Ga₂O₃ single crystals by the Czochralski method », *Journal of Applied Physics*, vol. 131, n° 3, p. 031103, janv. 2022, doi: 10.1063/5.0076962.
- [44] J. Y. Tsao *et al.*, « Ultrawide-Bandgap Semiconductors: Research Opportunities and Challenges », *Adv. Electron. Mater.*, vol. 4, n° 1, p. 1600501, janv. 2018, doi: 10.1002/aelm.201600501.
- [45] M. Higashiwaki, « β -Ga₂O₃ material properties, growth technologies, and devices: a review », *AAPPS Bull.*, vol. 32, n° 1, p. 3, janv. 2022, doi: 10.1007/s43673-021-00033-0.
- [46] A. Biswas, A. Banerjee, A. Acharyya, et H. Inokawa, Éd., *Emerging Trends in Terahertz Engineering and System Technologies: Devices, Materials, Imaging, Data Acquisition and Processing*. Singapore: Springer Singapore, 2021. doi: 10.1007/978-981-15-9766-4.
- [47] E. Chikoidze *et al.*, « Enhancing the intrinsic p-type conductivity of the ultra-wide bandgap Ga₂O₃ semiconductor », *J. Mater. Chem. C*, vol. 7, n° 33, p. 10231-10239, 2019, doi: 10.1039/C9TC02910A.
- [48] A. Kumar, S. Singh, et D. Shukla, « Preparation Properties and Device Application of β -Ga₂O₃: A Review », *IJRASET*, vol. 10, n° 8, p. 360-374, août 2022, doi: 10.22214/ijraset.2022.46195.
- [49] « Doping and semiconductor characterizations », in *Power Electronics Device Applications of Diamond Semiconductors*, Elsevier, 2018, p. 99-189. doi: 10.1016/B978-0-08-102183-5.00002-9.
- [50] X. Liang, « Transition from Tubes to Sheets—A Comparison of the Properties and Applications of Carbon Nanotubes and Graphene », in

- Nanotube Superfiber Materials*, Elsevier, 2014, p. 519-568. doi: 10.1016/B978-1-4557-7863-8.00019-0.
- [51] M. Higashiwaki et S. Fujita, Éd., *Gallium Oxide: Materials Properties, Crystal Growth, and Devices*, vol. 293. in Springer Series in Materials Science, vol. 293. Cham: Springer International Publishing, 2020. doi: 10.1007/978-3-030-37153-1.
- [52] H. Cui *et al.*, « Tuning electrical conductivity of β -Ga₂O₃ single crystals by Ta doping », *Journal of Alloys and Compounds*, vol. 788, p. 925-928, juin 2019, doi: 10.1016/j.jallcom.2019.02.076.
- [53] S. Lee, K. Kaneko, et S. Fujita, « Homoepitaxial growth of beta gallium oxide films by mist chemical vapor deposition », *Jpn. J. Appl. Phys.*, vol. 55, n° 12, p. 1202B8, déc. 2016, doi: 10.7567/JJAP.55.1202B8.
- [54] R. M. Kotecha *et al.*, « Electrothermal Modeling and Analysis of Gallium Oxide Power Switching Devices », in *ASME 2019 International Technical Conference and Exhibition on Packaging and Integration of Electronic and Photonic Microsystems*, Anaheim, California, USA: American Society of Mechanical Engineers, oct. 2019, p. V001T06A017. doi: 10.1115/IPACK2019-6453.
- [55] D. Wang, H. Xiao, Y. Le, C. Luan, et J. Ma, « Effect of Ta doping on the properties of β -Ga₂O₃ heteroepitaxial films prepared on KTaO₃(100) substrates », *J Mater Sci: Mater Electron*, vol. 32, n° 3, p. 2757-2764, févr. 2021, doi: 10.1007/s10854-020-05015-w.
- [56] W. Mi, X. Du, C. Luan, H. Xiao, et J. Ma, « Electrical and optical characterizations of β -Ga₂O₃:Sn films deposited on MgO (110) substrate by MOCVD », *RSC Adv.*, vol. 4, n° 58, p. 30579, juill. 2014, doi: 10.1039/C4RA02479F.
- [57] « PHYS_2326_021709.ppt ».
- [58] « BREAKDOWN in SOLID DIELECTRICS1.pdf ».
- [59] R. Kotecha, W. Metzger, B. Mather, S. Narumanchi, et A. Zakutayev, « Modeling and Analysis of Gallium Oxide Vertical Transistors », *ECS J. Solid State Sci. Technol.*, vol. 8, n° 7, p. Q3202-Q3205, 2019, doi: 10.1149/2.0401907jss.
- [60] R. Singh *et al.*, « The dawn of Ga₂O₃ HEMTs for high power electronics - A review », *Materials Science in Semiconductor Processing*, vol. 119, p. 105216, nov. 2020, doi: 10.1016/j.mssp.2020.105216.
- [61] « [29] metal-semiconductor field-effect transistors on single-crystal.pdf ».
- [62] J. Ballestín-Fuertes, J. Muñoz-Cruzado-Alba, J. F. Sanz-Osorio, et E.

- Laporta-Puyal, « Role of Wide Bandgap Materials in Power Electronics for Smart Grids Applications », *Electronics*, vol. 10, n° 6, p. 677, mars 2021, doi: 10.3390/electronics10060677.
- [63] T.-H. Yang *et al.*, « Temperature-dependent electrical properties of β -Ga₂O₃ Schottky barrier diodes on highly doped single-crystal substrates », *J. Semicond.*, vol. 40, n° 1, p. 012801, janv. 2019, doi: 10.1088/1674-4926/40/1/012801.
- [64] S. O. Kasap et P. Capper, Éd., *Springer handbook of electronic and photonic materials*. New York: Springer, 2006.
- [65] S. J. Pearton, S. Oh, S. Kim, J. Kim, et F. Ren, « Exfoliated and bulk β -gallium oxide electronic and photonic devices », *Science Talks*, vol. 1, p. 100001, mars 2022, doi: 10.1016/j.sctalk.2022.100001.
- [66] « Wang_B_T_2022.pdf ».
- [67] L. Dong, R. Jia, B. Xin, B. Peng, et Y. Zhang, « Effects of oxygen vacancies on the structural and optical properties of β -Ga₂O₃ », *Sci Rep*, vol. 7, n° 1, p. 40160, janv. 2017, doi: 10.1038/srep40160.
- [68] J. Zhou, H. Chen, K. Fu, et Y. Zhao, « Gallium oxide-based optical nonlinear effects and photonics devices », *Journal of Materials Research*, vol. 36, n° 23, p. 4832-4845, déc. 2021, doi: 10.1557/s43578-021-00397-x.
- [69] M. Baldini, Z. Galazka, et G. Wagner, « Recent progress in the growth of β -Ga₂O₃ for power electronics applications », *Materials Science in Semiconductor Processing*, vol. 78, p. 132-146, mai 2018, doi: 10.1016/j.mssp.2017.10.040.
- [70] J. Zhang *et al.*, « Growth and spectral characterization of β -Ga₂O₃ single crystals », *Journal of Physics and Chemistry of Solids*, vol. 67, n° 12, p. 2448-2451, déc. 2006, doi: 10.1016/j.jpcs.2006.06.025.
- [71] X. Li et J. Qin, « Beta-Gallium Oxide Nanoflags and Its Ultraviolet Photoluminescence Performances », *nanosci nanotechnol lett*, vol. 7, n° 2, p. 152-156, févr. 2015, doi: 10.1166/nnl.2015.1914.
- [72] V. I. Nikolaev, S. I. Stepanov, A. E. Romanov, et V. E. Bougrov, « Gallium oxide », in *Single Crystals of Electronic Materials*, Elsevier, 2019, p. 487-521. doi: 10.1016/B978-0-08-102096-8.00014-8.
- [73] N. P. Sepelak, « Master of Science in Mechanical Engineering ».
- [74] M. Xian *et al.*, « Asymmetrical Contact Geometry to Reduce Forward-Bias Degradation in β -Ga₂O₃ Rectifiers », *ECS J. Solid State Sci. Technol.*, vol. 9, n° 3, p. 035007, janv. 2020, doi: 10.1149/2162-8777/ab7b44.
- [75] L. Sang, M. Liao, et M. Sumiya, « A Comprehensive Review of Semiconductor Ultraviolet Photodetectors: From Thin Film to One-

- Dimensional Nanostructures », *Sensors*, vol. 13, n° 8, p. 10482-10518, août 2013, doi: 10.3390/s130810482.
- [76] J. Xu, W. Zheng, et F. Huang, « Gallium oxide solar-blind ultraviolet photodetectors: a review », *J. Mater. Chem. C*, vol. 7, n° 29, p. 8753-8770, 2019, doi: 10.1039/C9TC02055A.
- [77] Y.-C. Chen *et al.*, « Self-powered diamond/ β -Ga₂O₃ photodetectors for solar-blind imaging », *J. Mater. Chem. C*, vol. 6, n° 21, p. 5727-5732, 2018, doi: 10.1039/C8TC01122B.
- [78] Y. Qin *et al.*, « Review of deep ultraviolet photodetector based on gallium oxide », *Chinese Phys. B*, vol. 28, n° 1, p. 018501, janv. 2019, doi: 10.1088/1674-1056/28/1/018501.
- [79] Y. G. Wang *et al.*, « High Performance β -Ga₂O₃ vertical Schottky Barrier Diodes », in *2020 17th China International Forum on Solid State Lighting & 2020 International Forum on Wide Bandgap Semiconductors China (SSLChina: IFWS)*, Shenzhen, China: IEEE, nov. 2020, p. 224-227. doi: 10.1109/SSLChinaIFWS51786.2020.9308713.
- [80] D. Kaur et M. Kumar, « A Strategic Review on Gallium Oxide Based Deep-Ultraviolet Photodetectors: Recent Progress and Future Prospects », *Adv. Optical Mater.*, vol. 9, n° 9, p. 2002160, mai 2021, doi: 10.1002/adom.202002160.
- [81] S. Oh, Y. Jung, M. A. Mastro, J. K. Hite, C. R. Eddy, et J. Kim, « Development of solar-blind photodetectors based on Si-implanted β -Ga₂O₃ », *Opt. Express*, vol. 23, n° 22, p. 28300, nov. 2015, doi: 10.1364/OE.23.028300.
- [82] T. He *et al.*, « Solar-blind ultraviolet photodetector based on graphene/vertical Ga₂O₃ nanowire array heterojunction », *Nanophotonics*, vol. 7, n° 9, p. 1557-1562, sept. 2018, doi: 10.1515/nanoph-2018-0061.
- [83] L. Huang *et al.*, « Self-powered solar-blind ultraviolet photodetector based on α -Ga₂O₃ nanorod arrays fabricated by the water bath method », *Opt. Mater. Express*, vol. 11, n° 7, p. 2089, juill. 2021, doi: 10.1364/OME.431377.
- [84] L. Su, W. Yang, J. Cai, H. Chen, et X. Fang, « Self-Powered Ultraviolet Photodetectors Driven by Built-In Electric Field », *Small*, vol. 13, n° 45, p. 1701687, déc. 2017, doi: 10.1002/smll.201701687.
- [85] T. Tut, « PHOTODETECTORS WITH PERFORMANCES EXCEEDING THE PMTS ».
- [86] A. S. Pratiyush, S. Krishnamoorthy, R. Muralidharan, S. Rajan, et D. N. Nath, « Advances in Ga₂O₃ solar-blind UV photodetectors », in *Gallium*

- Oxide*, Elsevier, 2019, p. 369-399. doi: 10.1016/B978-0-12-814521-0.00016-6.
- [87] R. A. Miller, H. So, T. A. Heuser, et D. G. Senesky, « High-temperature Ultraviolet Photodetectors: A Review ».
- [88] N. Nasiri et A. Tricoli, « Nanomaterials-based UV photodetectors », in *Industrial Applications of Nanomaterials*, Elsevier, 2019, p. 123-149. doi: 10.1016/B978-0-12-815749-7.00005-0.
- [89] C. Xie *et al.*, « Recent Progress in Solar-Blind Deep-Ultraviolet Photodetectors Based on Inorganic Ultrawide Bandgap Semiconductors », *Adv Funct Materials*, vol. 29, n° 9, p. 1806006, févr. 2019, doi: 10.1002/adfm.201806006.
- [90] A. Perez-Tomas, E. Chikoidze, et D. J. Rogers, « A walk on the frontier of energy electronics with power ultra-wide bandgap oxides and ultra-thin neuromorphic 2D materials », in *Oxide-based Materials and Devices XII*, F. H. Teherani, D. C. Look, et D. J. Rogers, Éd., Online Only, United States: SPIE, avr. 2021, p. 63. doi: 10.1117/12.2590747.
- [91] L.-Y. Jian, H.-Y. Lee, et C.-T. Lee, « Ga₂O₃-based p-i-n solar blind deep ultraviolet photodetectors », *J Mater Sci: Mater Electron*, vol. 30, n° 9, p. 8445-8448, mai 2019, doi: 10.1007/s10854-019-01163-w.
- [92] A. Di Bartolomeo, « Graphene Schottky diodes: An experimental review of the rectifying graphene/semiconductor heterojunction », *Physics Reports*, vol. 606, p. 1-58, janv. 2016, doi: 10.1016/j.physrep.2015.10.003.
- [93] Biskra, « أوكسيد الغاليوم », جامعة محمد خيضر (Ga₂O₃) خ. بن كحول, « محاكاة تأثير وصلة شوتكي لثنائية من 2021. [En ligne]. Disponible sur: <http://archives.univ-biskra.dz/browse?type=author&value=%D8%A8%D9%86+%D9%83%D9%8A%D8%AD%D9%88%D9%84+%D8%AE%D8%A7%D9%84%D8%AF>
- [94] G. S. Korotchenkov, Éd., *Handbook of II-VI semiconductor-based sensors and radiation detectors. Vol. 3, Sensors, biosensors and radiation detectors*. Cham: Springer, 2023.
- [95] M. Ochoa Gómez, « TCAD Modelling, simulation and characterization of III-V multijunction solar cells », PhD Thesis, Universidad Politécnica de Madrid, 2018. doi: 10.20868/UPM.thesis.51571.
- [96] A. Djefal, « Study of the substitution possibility of Pb by Sn in perovskite solar cell », Mohamed Khider University, Biskra. [En ligne]. Disponible sur: <http://archives.univ-biskra.dz/handle/123456789/21744>
- [97] M. S. Nouredine, M. M. Afak, M. S. Abdelkadar, M. B. Abderahmane, M. Amjad, et U. Biskra, « Etude des Transistors couches minces (TFTs) à

- base d'alliages des oxydes amorphes d'In, Sn et Zn. Study of thin film transistors (TFTs) based on In, Sn and Zn amorphous oxides alloys ».
- [98] M. Labeled *et al.*, « Physical Operations of a Self-Powered IZTO/ β -Ga₂O₃ Schottky Barrier Diode Photodetector », *Nanomaterials*, vol. 12, n° 7, p. 1061, mars 2022, doi: 10.3390/nano12071061.
- [99] Y. D. Ko et Y. S. Kim, « Room temperature deposition of IZTO transparent anode films for organic light-emitting diodes », *Materials Research Bulletin*, vol. 47, n° 10, p. 2800-2803, oct. 2012, doi: 10.1016/j.materresbull.2012.04.089.
- [100] R. Cherroun *et al.*, « Study of a Solar-Blind Photodetector Based on an IZTO/ β -Ga₂O₃/ITO Schottky Diode », *J. Electron. Mater.*, vol. 52, n° 2, p. 1448-1460, févr. 2023, doi: 10.1007/s11664-022-10081-3.
- [101] « atlas_user_manual.pdf ».
- [102] S. M. Sze et K. K. Ng, *Physics of semiconductor devices*, 3^e éd. Hoboken, NJ, USA: John Wiley & Sons, 2006.
- [103] B. R. Tak, M. Garg, A. Kumar, V. Gupta, et R. Singh, « Gamma Irradiation Effect on Performance of β -Ga₂O₃ Metal-Semiconductor-Metal Solar-Blind Photodetectors for Space Applications », *ECS J. Solid State Sci. Technol.*, vol. 8, n° 7, p. Q3149-Q3153, 2019, doi: 10.1149/2.0291907jss.

Abstract:

In recent years, the solar-blind photodetectors based on β -Ga₂O₃ are attractive due to their simple fabrication process and its photodetection performance. Our study is about InZnSnO₂ (IZTO)/ β -Ga₂O₃ solar blind Schottky barrier diode photodetector (PhD). It was realized successfully by Silvaco-Atlas simulation. The first part of our study is to expose this device to light source (LED) (255 nm, 385 nm and 500 nm) with a power density of 1 mW/cm² and it was simulated J-V, responsivity, response time characteristics and compared with measurement. In the second part of our study is study the effect of reducing trap densities (deep and shallow trap) on performance of the photodetector. When we decrease in deep trap densities, we notice that the saturation zone current is decrease. However, when the decreasing shallow traps densities, we notice that The decay time was shorter (~ 0.019 s for $E_T = 0.55$ eV). However, it was be slower when the trap is deeper because we find his value for $E_T = 0.74$ eV is ~ 0.38 s and for $E_T = 1.04$ eV is ~ 0.099 s. So, this indicates that the shallowest traps had the dominant influence ($E_T = 0.55$ eV) on the persistent photoconductivity phenomenon. Furthermore, with decreasing trap densities, this PhD can be considered as a self-powered solar-blind photodiode (SBPhD).

Key words : Beta gallium oxide, solar blind photodetector, Silvaco-Atlas.

